HER2 recruits AKT1 to disrupt STING signalling and suppress antiviral defence and antitumour immunity

Shiying Wu[1,8], Qian Zhang[1,2,8], Fei Zhang[1,8], Fansen Meng[1,2], Shengduo Liu[1], Ruyuan Zhou[1], Qingzhe Wu[1], Xinran Li[1], Li Shen[1], Jun Huang[1], Jun Qin[3], Songying Ouyang[4], Zongping Xia[5], Hai Song[1], Xin-Hua Feng[1,6], Jian Zou[7] and Pinglong Xu[1,2]*

Sensing cytosolic DNA through the cGAS–STING pathway constitutes a widespread innate immune mechanism to monitor cellular damage and microbial invasion. Evading this surveillance is crucial in tumorigenesis, but the process remains largely unexplored. Here, we show that the receptor tyrosine kinase HER2 (also known as ErbB-2 or Neu) potently inhibits cGAS–STING signalling and prevents cancer cells from producing cytokines, entering senescence and undergoing apoptosis. HER2, but not EGFR, associates strongly with STING and recruits AKT1 (also known as PKB) to directly phosphorylate TBK1, which prevents the TBK1–STING association and TBK1 K63-linked ubiquitination, thus attenuating STING signalling. Unexpectedly, we observed that DNA sensing robustly activates the HER2–AKT1 axis, resulting in negative feedback. Accordingly, genetic or pharmacological targeting of the HER2–AKT1 cascade augments damage-induced cellular senescence and apoptosis, and enhances STING-mediated antiviral and antitumour immunity. Thus, our findings reveal a critical function of the oncogenic pathway in innate immune regulation and unexpectedly connect HER2–AKT1 signalling to the surveillance of cellular damage and antitumour immunity.

Metazoans recognize conserved pathogen-associated molecular patterns and damage-associated molecular patterns by innate immune sensing mechanisms to fight against pathogen infection and maintain tissue homeostasis. Cytosolic DNA sensors such as cGAS[1,2] are essential components in these surveillance systems, particularly for sensing damage that causes the release of DNA fragments from the nucleus or mitochondria into the cytosol[3–5]. Recognition of cytosolic DNA by cGAS leads to the translocation of endoplasmic reticulum (ER)-associated STING (also known as MITA or ERIS)[6–8] and the assembly of the STING signalosome[9–12], which is driven by the second messenger 2'3'-cGAMP[1]. TBK1 and/or IKKε kinases then phosphorylate IRF3 in the STING signalosome and mobilize IRF3 to dimerize, translocate to the nucleus and function as a transcription factor, in coordination with the simultaneously activated NF-κB[3–5], to drive the expression of type I interferons (IFNs)[13,14]. The subsequent and coordinated transcriptome of IFN-stimulated genes (ISGs) thus restricts microbial infection, modulates adaptive immunity and initializes tissue regeneration[3–5].

Exaggerated or aberrant responses to viral or native nucleic acids and subsequent excess production of IFNs trigger autoimmune and autoinflammatory diseases[15,16]. In addition to its role in IFN and cytokine production, the cGAS–STING pathway, when activated, frequently leads to cellular senescence[17–19] and boosts antitumour immunity in the tumour setting[20–22]. In contrast, aberrant DNA fragments are ubiquitous in various cancer cells due to abnormal chromosome structure and genome instability[23,24], which can be sensed by cGAS–STING signalling in both the cytosol and micronuclei[17,19,23,24]. STING agonists have thus emerged as an effective immune adjuvant in the treatment of infectious diseases or cancer[21,25,26]. Evading damage surveillance is therefore indispensable in tumorigenesis. Although defects in key molecules of cytosolic DNA sensing account for partial causations in the observed evasion[3,5,17,24], the cytosolic DNA sensing pathway seems to be intact in a substantial subset of cancers. Therefore, elucidating the cellular mechanism underlying the loss of cytosolic DNA sensing is valuable both to the understanding of tumorigenesis and developing treatments.

The assembly of the STING signalosome involves the tenuous translocation of STING from the ER to the Golgi apparatus and perinuclear microsome[9–12]. At present, the components, cellular localization and precise mechanism involved in the initiation and activation of the STING signalosome are still unclear. TBK1, the central kinase of the STING signalosome[27,28], along with IKKε, serves as a key regulator of apoptosis, autophagy and inflammatory responses[3–5,29]. Nucleic-acid-sensing-induced activation of TBK1 is a complicated process regulated by intermolecular trans-autophosphorylation and K63-linked ubiquitination[30], and is subjected to elaborate regulatory processes[31,32] and interrelated with

[1]MOE Laboratory of Biosystems Homeostasis and Protection and Innovation Center for Cell Signaling Network, Life Sciences Institute, Zhejiang University, Hangzhou, China. [2]Department of Hepatobiliary and Pancreatic Surgery and Zhejiang Provincial Key Laboratory of Pancreatic Disease, The First Affiliated Hospital, School of Medicine, Zhejiang University, Hangzhou, China. [3]CAS Key Laboratory of Tissue Microenvironment and Tumor, Center for Excellence in Molecular Cell Science, Shanghai Institute of Nutrition and Health, Chinese Academy of Sciences, Shanghai, China. [4]The Key Laboratory of Innate Immune Biology of Fujian Province, Biomedical Research Center of South China, College of Life Sciences, Fujian Normal University, Fuzhou, China. [5]Translational Medicine Center, The First Affiliated Hospital, Zhengzhou University, Zhengzhou, China. [6]Michael E. DeBakey Department of Surgery and Department of Molecular and Cellular Biology, Baylor College of Medicine, Houston, TX, USA. [7]Eye Center of the Second Affiliated Hospital, Institute of Translational Medicine, School of Medicine, Zhejiang University, Hangzhou, China. [8]These authors contributed equally: Shiying Wu, Qian Zhang, Fei Zhang. *e-mail: xupl@zju.edu.cn

environmental cues[33]. We recently reported that YAP/TAZ, the key effectors of Hippo signalling, and the ion-metal phosphatase PPM1A are potent suppressors of TBK1 (refs. [33,34]). The non-receptor tyrosine kinases LCK, HCK and FGR negatively regulate TBK1 by directly phosphorylating tyrosine residues[35]. Despite the critical roles of TBK1/IKKε activation and termination in many aspects of cell biology and contexts of diseases, the precise mechanism is still poorly understood.

HER2 (also known as ErbB-2 or Neu) is a ligand-independent receptor tyrosine kinase (RTK) functioning as a signalling mediator of various other RTKs. Despite its ubiquitous expression, HER2 is commonly altered, such as amplification and activating deletions, in metastatic breast, prostate and ovarian cancers[36,37]. Notably, treatments inhibiting HER2, such as trastuzumab (Herceptin), induce robust lymphocyte tumour infiltration and its efficacy depends heavily on immune regulation[38]. Mounting evidence also suggests that the innate immune system—particularly IFNs and ISGs—is involved in the immunotherapy or chemotherapy effects of blocking HER2[39,40] and neutralization of IFN receptor 1 (IFNAR1) abrogates the therapeutic efficacy of anti-HER2 monoclonal antibodies[41,42]. These interesting findings thus imply the involvement of HER2 in innate immune regulation, although the underlying mechanism(s) are unknown.

Here, we found that HER2 is a natural and potent inhibitor of cytosolic DNA sensing, and revealed that HER2-mediated suppression of cGAS–STING signalling is vital to prevent cancer cells from entering senescence and undergoing apoptosis. HER2 associates strongly with STING through its intracellular domain (ICD) to recruit AKT1 to STING, which directly phosphorylates TBK1 at S510 to impede the TBK1–STING association and TBK1 K63-linked ubiquitination, thus attenuating DNA sensing. This work reveals a critical function of HER2 in innate immune sensing and connects an oncogenic pathway to cellular damage surveillance and antitumour immunity.

Results

HER2 suppresses cGAS–STING signalling to dampen cytosolic DNA sensing. To systematically evaluate tyrosine kinases in cytosolic DNA sensing, we employed a tyrosine kinome complimentary DNA library and assessed the role of individual kinases in the regulation of STING signalling. Reporter screening revealed that HER2, a ubiquitously expressed RTK of the HER/ERBB family, markedly impeded STING signalling (Fig. 1a). HER2-mediated inhibition seemed to be specific, as other HER-family members showed marginal effects on STING signalling despite their activation

profile (Fig. 1b,c and Supplementary Fig. 1a). Intriguingly, an activating mutation of EGFR (L858R) potentiated the activation of TBK1 regardless of the HER2 levels (Supplementary Fig. 1b,c). HER2 suppressed STING- or TBK1-initiated signalling in a dose-dependent manner but failed to suppress the activated IRF3 (5SD) (Fig. 1d and Supplementary Fig. 1d,e). Notably, the ICD of HER2, the expression of which is often observed and elevated in cancers, was sufficient and effective in mediating this suppression (Fig. 1e and Supplementary Fig. 1f). These observations suggest that HER2 is a potential inhibitor of STING signalling.

To further confirm this observation, we generated cell lines with inducible HER2 expression using the Tet-On system from human gut epithelial cancer cells (DLD1), mouse normal mammary gland epithelial cells (NMuMG) and mouse embryonic fibroblasts (MEFs). Both immunoblotting of TBK1 activation and messenger RNA expression of downstream ISGs showed that HER2 induction strongly suppressed cytosolic DNA sensing when stimulated either by cytosolic exposure of a DNA analogue (Fig. 1f) or by direct activation of STING with its natural agonist cGAMP[1] (Fig. 1g). This potent and specific effect of HER2 suggests that HER2 exerts a biological function in innate immune regulation.

Small molecule targeting or genetic ablation of HER2 potentiates cytosolic DNA sensing. Small molecule inhibitors were then employed to verify the specific role of endogenous HER2. We detected a dramatic boost in DNA sensing in HEK293 cells, measured with an IRF3-responsive IFN-sensitive response element (ISRE) or IFNβ reporter, following the addition of the HER2 inhibitors lapatinib and ARRY-380 (tucatinib; Fig. 1h and Supplementary Fig. 1g). The HER2 inhibitors also potentiated the STING-dependent activation of endogenous TBK1 (Fig. 1i and Supplementary Fig. 1h). In contrast, small molecules targeting EGFR/HER1, such as WZ4002 or icotinib, showed no observable effect on STING signalling (Fig. 1h and Supplementary Fig. 1h). Notably, targeting HER2 markedly potentiated STING signalling in the HER2-driven BT474 and SKBR-3 tumour cell lines (Fig. 1j and Supplementary Fig. 1i) and in human peripheral blood mononuclear cells (PBMCs; Fig. 1k) regardless of stimulations with cGMAP, cytosolic DNA analogues, genomic DNA or viral DNA (Fig. 1j–l and Supplementary Fig. 1i,j). These data suggest that HER2 activity is a key factor in determining cytosolic sensing of DNA.

We next generated HER2-knockout cells using a clustered regularly interspaced short palindromic repeats (CRISPR)-mediated strategy in DLD1, NMuMG and human colorectal epithelial cancer (HCT116) cells. HER2-knockout in DLD1 cells substantially

Fig. 1 | HER2 suppresses cytosolic DNA sensing. a, Screening of the tyrosine kinome cDNA library revealed HER2 to be a strong suppressor of STING signalling. A luciferase-reporter assay with an IRF3-responsive ISRE promoter stimulated by STING coexpression was used in HEK293 cells. **b,c**, STING activation, as indicated by an ISRE reporter (**b**; HEK293 cells) or phospho (p)-TBK1(S172) (**c**; HCT116 cells), was profoundly inhibited following coexpression with HER2 but not with other ERBB family RTKs. **d,e**, HER2, but not EGFR, inhibited TBK1 in a dose-dependent manner, as indicated by the IRF3-responsive IFNβ reporter or TBK1 activation in HEK293 cells (**d**; n = 4 independent experiments); the intracellular domain of HER2 markedly inhibited TBK1 activation (**e**). **f**, Cytosolic DNA sensing simulated by the cytosolic exposure of DNA analogues poly(dA:dT) was attenuated by inducing HER2 expression in MEFs using the Tet-On system. **g**, cGAMP-induced ISG mRNA expression was completely blocked by inducible HER2 expression in DLD1 cells. **h**, HER2 inhibitors, lapatinib and ARRY-380, but not EGFR inhibitors, WZ4002 and icotinib, substantially potentiated STING signalling in HEK293 cells. **i,j**, Inhibition of HER2 by lapatinib or ARRY-380 profoundly enhanced the TpdAdT-induced activation of endogenous TBK1, which was absent in STING-knockout DLD1 cells (**i**); Lapatinib potentiated TpdAdT- or cGAMP-induced STING signalling in the HER2-driven tumour lines BT474 (**j**, left) and SKBR-3 (**j**, right). l.e., longer exposure. **k,l**, The hydroxyurea- and cGAMP-stimulated cytosolic DNA sensing in human PBMCs (**k**), and sensing of DNA virus HSV-1 in NMuMG cells (**l**) were potently boosted by HER2 inhibition. l.s., lipid soluble. **m**, Enhanced cytosolic DNA sensing in HER2-knockout DLD1 cells was detected, but the opposite effect was observed in HER2-reconstituted cells; activation of EGFR signalling by ligand EGF somewhat potentiated DNA innate sensing with or without HER2. **n,o**, HER2 ablation in NMuMG (**o**) or HCT116 (**n**) cells dramatically enhanced STING signalling, as assessed by determining the mRNA expression levels of *IFNβ* and ISGs; this was reversed following the reintroduction of HER2 expression (**o**). **p**, Lapatinib failed to enhance cytosolic DNA sensing in NMuMG cells without HER2. Unless otherwise specified, n = 3 independent experiments; the mean ± s.e.m. is shown. *P* values are indicated; analysis of variance (ANOVA) test with Bonferroni correction. Unprocessed images of the blots are shown in Supplementary Fig. 8. The statistics source data are provided in Supplementary Table 1. Dox, doxycycline; TpdAdT, transfected poly(dA:dT); HU, hydroxyurea; WT, wild type; IP, immunoprecititation and n.s., not significant.

enhanced cytosolic DNA sensing, which was rescued by HER2 reconstitution (Fig. 1m and Supplementary Fig. 1k,l). In contrast, activation of EGFR and HER3/HER4 signalling by their

ligands failed to arrest STING signalling, suggesting that regulation does not occur through the heterodimers formed between HER2 and HER-family RTKs. HER2-knockout in HCT116 and
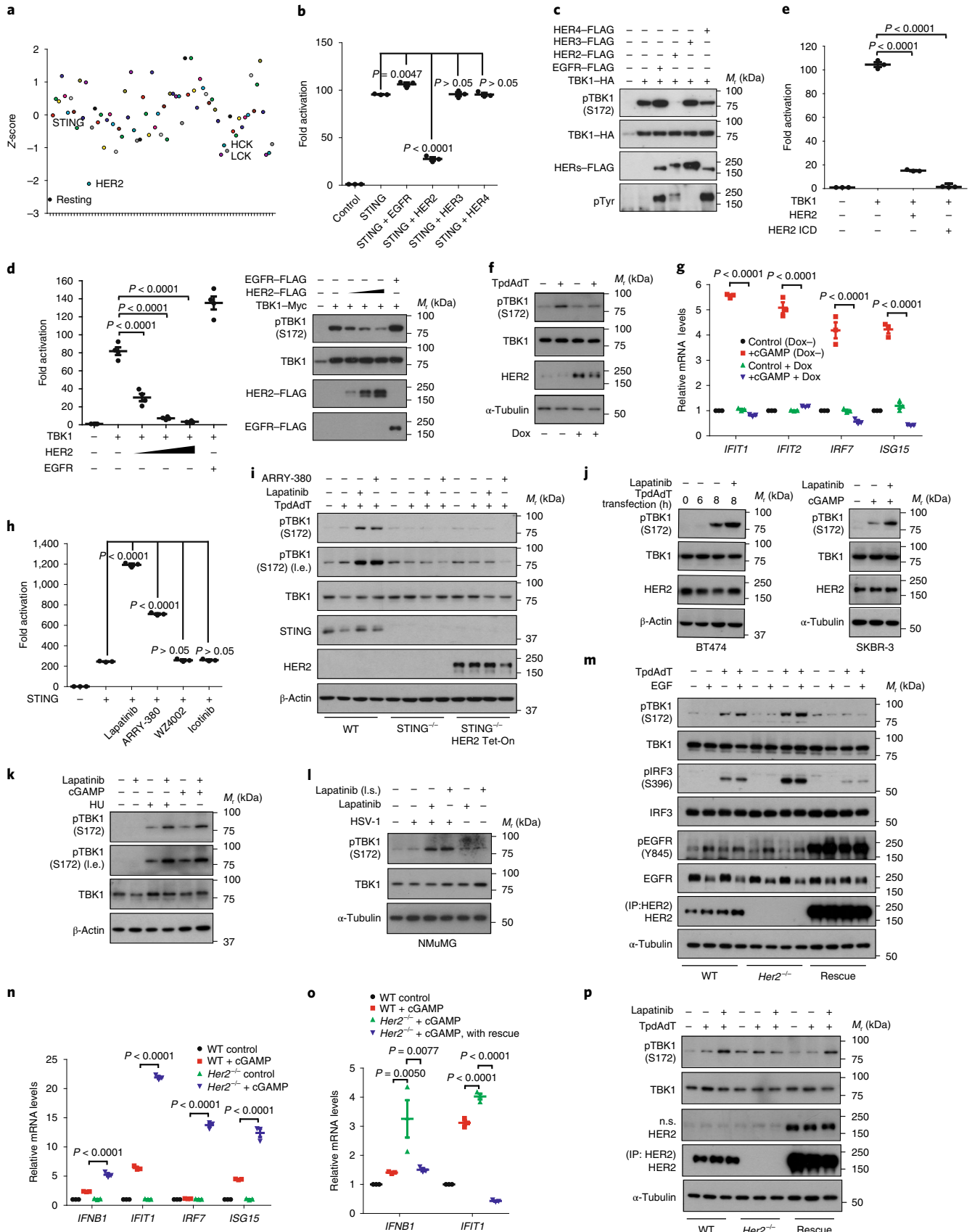
NMuMG cells (Supplementary Fig. 1m) also markedly enhanced the mRNA expression of ISGs following cGAMP stimulation (Fig. 1n,o). HER2 reconstitution restored this suppressive phenotype, whereas lapatinib failed to further enhance cytosolic DNA sensing in *Her2*^{−/−} cells (Fig. 1p). In addition, HER2 depletion in BT474 cells effectively boosted STING signalling (Supplementary Fig. 1n). These consistent observations suggest that endogenous HER2 is a natural and potent suppressor of cytosolic DNA sensing in cells of various origins.

HER2 associates with STING and disrupts the STING signalosome. Following cGAMP treatment, STING aggregated into puncta and translocated from the ER to the Golgi apparatus (Fig. 2a and Supplementary Fig. 2a,b), reflecting the process for the assembly of the STING signalosome. Interestingly, aggregation of STING was sensitized in the presence of lapatinib, leading to a more condensed distribution of STING (Fig. 2a and Supplementary Fig. 2b) and a higher degree of aggregation on the Golgi apparatus in the late stage (Supplementary Fig. 2a). In contrast, expression of the HER2 ICD impeded this STING aggregation (Fig. 2b). These data suggest that HER2 disrupts the assembly of the STING signalosome.

We detected a robust association between endogenous HER2 and STING in gut epithelial cells, which was partially disrupted when STING was stimulated for extensive time periods by cGAMP or HER2 was inhibited by lapatinib (Fig. 2c). This strong association between STING and HER2, but not EGFR, was also observed when HER2 and STING were cotransfected into HEK293 cells (Supplementary Fig. 2c,d). Immunofluorescence under confocal microscopy unexpectedly revealed that endogenous HER2 in BT474 cells or induced HER2 in DLD1 cells was substantially redistributed—from disseminated along the plasma membrane and ER to forming puncta at the ER compartments—following cGAMP stimulation and overlapped substantially with endogenous STING (Fig. 2d,e and Supplementary Fig. 2e,f). In contrast, lapatinib restricted the cellular localization of HER2 to the plasma membrane (Fig. 2e and Supplementary Fig. 2f–h), probably preventing the HER2–STING interaction. We also observed that a small subset of HER2 puncta was associated with Golgi markers following extended cGAMP stimulation (Supplementary Fig. 2g,h). Domain mapping analysis revealed that the C-terminal domain (amino-acid residues 139–379) of STING and the intact ICD of HER2 were necessary and sufficient for HER2 recruitment (Fig. 2f and Supplementary Fig. 2i). The C-terminal tail of STING (residues 340–379), which is involved in the interaction with TBK1 and IRF3 recruitment[27,28], was also indispensable for their interaction. These interesting observations demonstrate the physical and functional interaction between STING and HER2, occurring mostly in ER compartments and partially in the Golgi apparatus. The underlying mechanism for the cGAMP-stimulated redistribution of HER2 is of interest but awaits future investigation.

The negative regulation of HER2 on the STING signalosome was further verified by surveillance of the interaction of TBK1 with its adaptors STING and TRAF6 and the substrate IRF3. HER2 markedly disrupted the association between STING and TBK1, which was exclusively dependent on HER2 activity (Fig. 2g). As expected, the HER2 ICD was sufficient to disrupt the STING–TBK1 complex (Fig. 2h). HER2, but not EGFR, also impeded the association of TBK1 with IRF3, the key signalling effector (Fig. 2i). Similarly, the association of TBK1 with the TRAF family E3 ligase TRAF6 (refs. [43,44]) was attenuated by activated HER2 (Fig. 2j). K63-linked ubiquitination of TBK1, which is catalysed by the TRAF family and/or other E3 ligases and is important for TBK1 activation[43,45–49], was severely impaired by HER2 (Fig. 2k). Furthermore, we found that HER2 blocked the *cis*-K63 ubiquitination of TRAF6 and thus its activation (Supplementary Fig. 2j). These observations suggest that HER2 binds STING to prevent the assembly of the STING signalosome, relying on its kinase activity.

The HER2–AKT1 axis is activated and critical for HER2-mediated suppression. Unlike what was previously reported for the tyrosine kinase LCK[35], we failed to detect that HER2 directly modified the tyrosine residue(s) on TBK1, STING or TRAFs (Supplementary Fig. 3a,b). We thus evaluated the effect of downstream signalling cascades, including MAPK and PI$_3$K–AKT signalling, following HER2 activation. Strikingly, we noticed that infection with the DNA viruses HSV-1 and VacV or cytosolic exposure of DNA analogues induced a robust AKT1 activation in mouse peritoneal macrophages and human PBMCs (Fig. 3a–c and Supplementary Fig. 3c). AKT1 activation seemed to be caused by HER2 because HER2 was activated during DNA innate sensing (Supplementary Fig. 3d) and inhibition of HER2 abolished this AKT1 activation (Fig. 3a–c). Cytosolic exposure of DNA analogues in epithelial cells also activated AKT1 (Fig. 3d). The mechanism for DNA sensing-induced HER2 activation is currently unknown. In contrast to the dramatic effect of AKT inhibition by MK2206, inhibition of MEK1/2 kinases by U0126 did not reverse HER2-mediated TBK1 inhibition (Fig. 3e), suggesting that AKT kinases are at least partially involved in HER2-mediated suppression. Intriguingly, among the AKT members, only AKT1 had an inhibitory effect on TBK1 (Fig. 3f,g). Interestingly, a robust interaction between STING and AKT1 was only detected in the presence of HER2 (but not EGFR) and blocking of HER2 activity weakened this recruitment (Fig. 3h), indicating that HER2 recruits AKT1 to the STING signalosome. AKT1, but not AKT2 and AKT3, was effectively recruited to STING, which might be due to a higher affinity for HER2 (Fig. 3i). This observation may reflect the distinction between the role of AKT1 and AKT2 or AKT3 in STING signalling.

Fig. 2 | HER2 associates with STING and disrupts the assembly of the STING signalosome. a,b, STING aggregation (puncta) in response to cGAMP treatment was denser in the presence of lapatinib than in its absence at 2 h post cGAMP administration (**a**). The expression of the HER2 ICD prevented STING aggregation (**b**). **c**, Coimmunoprecipitation revealed a complex comprising endogenous STING and HER2 in DLD1 cells that was weakened by extended treatment with cGAMP or lapatinib. **d,e**, Immunofluorescence under confocal microscopy revealed the colocalization of endogenous HER2 and STING in the BT474 cell line within the puncta of STING formed by cGAMP stimulation (indicated by the arrows in **d**). A substantial localization change of endogenous HER2, from dispersive distribution along the plasma membrane and ER to the formation of puncta at the ER, following cGAMP stimulation was detected (indicated by the arrows in **e**). **e**, Lapatinib affected the cellular localization of HER2, which showed reduced distribution to the ER compartments. **f**, Coimmunoprecipitation assays of HER2 and STING truncations showed that the STING C-terminal domain (residues 139–379) is sufficient for their interaction. The deletion of the C-terminal tail of STING abrogated this interaction. Domains of STING and their corresponding amino acid position are depicted (bottom). TM, transmembrane region. **g**, The interaction between STING and TBK1, an association that is key to the assembly of the STING signalosome, was completely disrupted in the presence of HER2. In contrast, inhibition of HER2 activity by lapatinib fully restored the association between STING and TBK1. **h**, The association between STING and TBK1 was completely disrupted by the ICD of HER2. **i,j**, HER2 impeded the association of TBK1 with its substrate IRF3 (**i**) and the adaptor/ubiquitin E3 ligase TRAF6 (**j**), which was prevented by lapatinib. The IRF3 2SA mutant was used to capture the weak association between TBK1 and IRF3. **k**, TBK1 K63-linked ubiquitination was abolished in the presence of HER2 but not EGFR. $n = 3$ independent experiments for all panels. The unprocessed images of the blots are shown in Supplementary Fig. 8. IB, immunoblotting; CTD, C-terminal domain; CTT, C-terminal tail and Ub, ubiquitin. Scale bars, 20 μm.

Furthermore, targeting AKT with MK2206 potentiated STING signalling (Fig. 3d and Supplementary Fig. 3e), albeit not as effectively as HER2 inhibition. Blocking AKT activity with MK2206 also impeded the ability of HER2 to disrupt the STING–TBK1 association (Fig. 3j), suggesting that AKT1 is important in the regulation of the STING signalosome. We then generated AKT1-knockout or
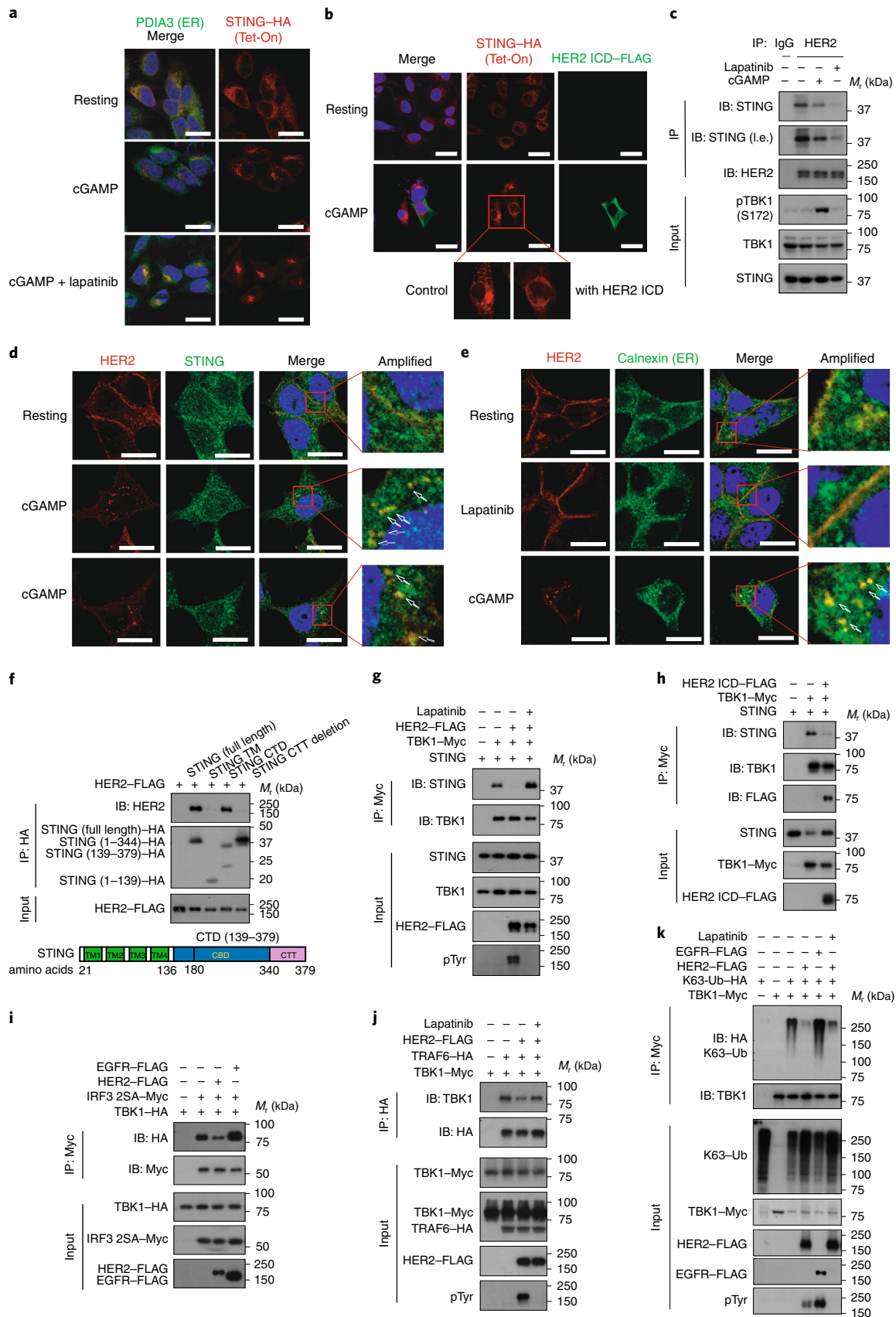
AKT2/AKT3-double knockout cells using CRISPR-based technology. Stronger STING signalling was detected in AKT1-null HEK293 cells (Fig. 3k). Importantly, HER2 expression failed to suppress TBK1 activation in the absence of AKT1 (Fig. 3l and Supplementary Fig. 3f) and HER2 was ineffective at attenuating K63-linked ubiquitination of TBK1 without AKT1 (Fig. 3m). AKT1 ablation not only improved TBK1 activation but also abrogated HER2-mediated regulation, which was recovered by expressing AKT1 ectopically (Fig. 3n). In contrast, double ablation of AKT2 and AKT3 did not abrogate HER2-mediated suppression (Supplementary Fig. 3g,h) and AKT family kinases seemed to not be involved in the EGFR L858R-induced potentiation of STING signalling and the TBK1–IRF3 interaction (Supplementary Fig. 3i,j). These data suggest that HER2 selectively recruits AKT1 to the STING signalosome to effectively suppress STING signalling.

AKT1 phosphorylates TBK1 at S510 to impede the assembly of the STING signalosome. AKT1-mediated modifications on key components of DNA innate sensing were then evaluated. By utilizing the AKT substrate antibody (phospho-RXXS*/T*), we detected a strong AKT1-mediated phosphorylation on TBK1 but not on cGAS, STING, TRAFs, IRF3, RIG-I or MAVS in HEK293 cells (Fig. 4a and Supplementary Fig. 4a). We also generated HCT116 cells with a knock-in of a FLAG tag to endogenous TBK1 using CRISPR-based strategy. AKT-directed phosphorylation of endogenous TBK1 was clearly seen via enrichment in anti-FLAG immunoprecipitation (Fig. 4b). MK2206 abolished both AKT activation and this TBK1 modification (Fig. 4c). Notably, this phospho-TBK1(AKT) signal completely disappeared when TBK1 was expressed in AKT1-knockout cells (second lane, Fig. 4d) and, in vitro, purified TBK1 was directly modified by AKT1, which was separately expressed and isolated (Fig. 4d). These data suggest that TBK1 is a substrate of AKT1.

Using mass spectrometry analysis, we observed that AKT1 altered a myriad of TBK1 phosphorylatable residues (Fig. 4e), thus implying a potential change in the TBK1 structure and function. Interestingly, a cluster of residues in the first coiled-coil domain (CCD1) of TBK1, near the amino-acid residues 499–527, is abundantly phosphorylated (designated the phosphorylation-rich motif). In particular, a dramatic increase of S510 phosphorylation was observed in the presence of active AKT1 (Supplementary Fig. 4b) along with a marked decrease in phosphorylation on the proximal residues in the phosphorylation-rich motif as well as on the key activation residue S172 (Fig. 4e).

The sequence proximal to S510 fits the known ATK1 substrate motif. Analysis with point mutations revealed that S510 is the major residue for AKT1-mediated modification, as mutating the S510 residue into alanine (S510A) or aspartate (S510D) completely
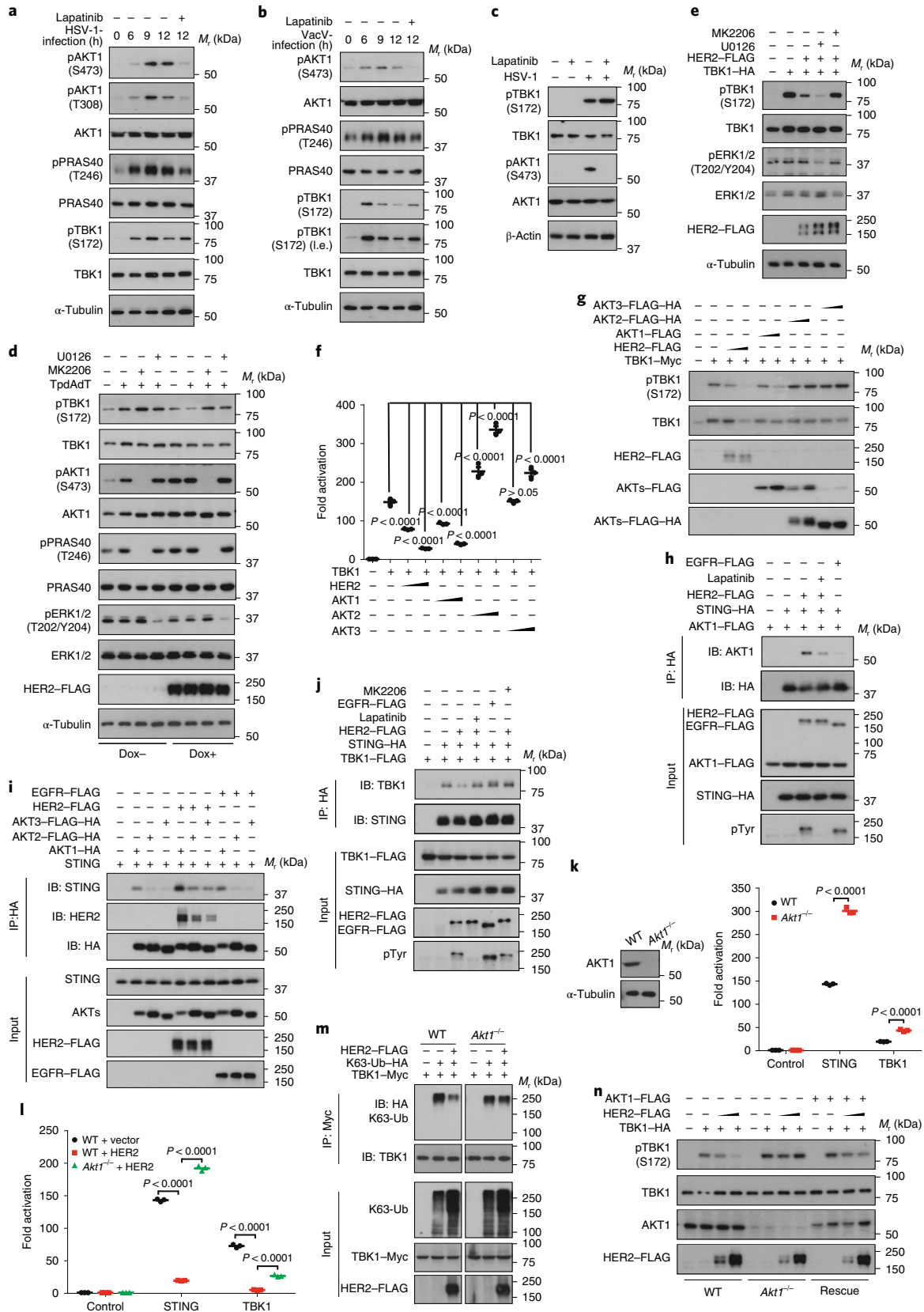
abolished AKT1-induced phosphorylation (Fig. 4f). As expected, the R507A mutation lost this AKT1-substrate signal, whereas the L505R mutation, which mimicked the preferred ATK1 recognition motif, further enhanced this already robust signal (Supplementary Fig. 4c). The phosphorylation state of the phosphorylation-rich motif seemed to facilitate the AKT1-mediated phosphorylation at S510 (Supplementary Fig. 4d). Notably, the S510A or 3TS/A TBK1 mutants, which had reduced AKT1-mediated phosphorylation (Supplementary Fig. 4d), showed higher kinase activity, whereas a TBK1-simulating AKT1-mediated modification (S510D + S499A) had compromised activation (Fig. 4g). Importantly, we observed a drastic decrease in the STING–TBK1 association (Fig. 4h) and a reduced interaction between TBK1 and IRF3 (Supplementary Fig. 4e) when constitutive AKT1-mediated TBK1 phosphorylation was mimicked, similar to the dose-dependent HER2 ICD-mediated abolishment of the STING–TBK1 interaction (Fig. 4i). In addition, AKT1 but not AKT2 or AKT3 selectively phosphorylated TBK1 in cells (Supplementary Fig. 4f). We further generated DLD1 cells with a S510A point mutagenesis knock-in to endogenous TBK1 by CRISPR-mediated genome editing (Supplementary Fig. 4g), which prevented AKT1-mediated modification (Fig. 4f). We then observed significantly enhanced activation of endogenous TBK1 and IRF3 (Fig. 4j) as well as more intense puncta of STING aggregation following cGAMP stimulation in these TBK1 S510A knock-in cells (Fig. 4k), illustrating a more efficient signalling cascade in the absence of interference from the HER2–AKT1 axis.

HER2 weakens the antiviral defence initiated by cytosolic DNA sensing. HER2 is ubiquitously expressed and cytosolic DNA sensing is critical for host defence against microbial pathogens such as DNA viruses. We thus evaluated the function of HER2 in innate antiviral immunity. Replication of the HSV-1 in NMuMG cells was measured by a green fluorescence protein (GFP) tag or luciferase integration into the viral genome, which revealed a dramatic downregulation of HSV-1 infection in the presence of the HER2 inhibitor or when HER2 expression was genetically ablated (Fig. 5a,b). In contrast, induced expression of HER2 boosted HSV-1 replication (Fig. 5c). As expected, the potentiation of HSV-1 infection by HER2 was dependent on STING expression (Fig. 5d and Supplementary Fig. 5a). HSV-1 infection in TBK1 S510A knock-in DLD1 cells revealed a marked enhancement of the cellular antiviral defence when AKT1-mediated TBK1 phosphorylation was blocked (Fig. 5e,f). Furthermore, to assess the physiological impacts of the HER2–AKT1 axis in antiviral immunity, we employed an HSV-1 corneal infection mice model[50]. HSV-1 infection resulted in the phenotypes of severe ocular disease, which was significantly alleviated by the ocular administration of lapatinib (Fig. 5g and Supplementary Fig. 5b),

Fig. 3 | The HER2–AKT1 axis is activated and required for HER2-mediated suppression of cytosolic DNA sensing. a,b, Robust signals for activation of PI₃K–AKT signalling were indicated following immunoblotting of phospho-AKT1 and phospho-PRAS40 in mouse peritoneal macrophages during infection with HSV-1 (**a**) and VacV (**b**). The ATK1-activation dynamics accompanied those of TBK1 but were abolished by lapatinib. **c,** Lapatinib treatment inhibited AKT1 phosphorylation but promoted TBK1 activation induced by HSV-1 in human PBMCs during infection. **d,** AKT1 was activated during cytosolic sensing of the DNA analogue (second lane) and after HER2 induction (fifth lane) in DLD1 cells. MK2206 treatment boosted TBK1 activation and partially rescued HER2-mediated suppression. **e,** The AKT inhibitor MK2206, but not the MEK1/2 inhibitor U0126, reversed the bulk of the HER2-mediated suppression of TBK1 activation. **f,g,** Suppression of TBK1 activation by AKT1, but not by AKT2 or AKT3, in HEK293 cells was detected through both the IRF3-responsive reporter assay (**f**) and immunoblotting for TBK1 activation (**g**). **h,** Coimmunoprecipitation assays revealed that AKT1 was recruited to the STING complex in the presence of HER2 but not EGFR. The blocking of HER2 activity with lapatinib prevented this recruitment. **i,** AKT1, but not AKT2 or AKT3, was effectively recruited to STING by HER2. **j,** The HER2-mediated disruption of the STING–TBK1 interaction was relieved by inhibiting AKT activity with MK2206 and blocking HER2 activity with lapatinib. Despite its robust activation, EGFR did not prevent the formation of the STING–TBK1 complex. **k,l,** Enhanced activation of STING and TBK1 was detected using a IRF3-responsive reporter assay in AKT1-knockout HEK293 cells generated by CRISPR-mediated genome editing (**k**); AKT1 ablation rescued most of the effects of HER2-mediated suppression on STING signalling (**l**). **m,** HER2-mediated attenuation of TBK1 K63-linked ubiquitination was partially relieved in AKT1-knockout cells. **n,** In addition to stronger TBK1 activation, HER2 failed to suppress TBK1 activation in *Akt1⁻/⁻* HEK293 cells, which was reversed when AKT1 expression was reconstituted. $n = 3$ independent experiments for all panels; the mean ± s.e.m. is shown. *P* values are indicated; ANOVA test with Bonferroni correction. The unprocessed images of the blots are shown in Supplementary Fig. 8. The statistics source data are provided in Supplementary Table 1.

with relieved disease scoring (Fig. 5h) and reduced viral load in the eyes (Fig. 5i). This observation suggests a key role of the HER2–AKT1 axis in antiviral immunity and implies a therapeutic potential against infectious diseases by targeting the HER2–AKT1 axis.

HER2 overcomes damage-induced cellular senescence and apoptosis. The emerging role of cytosolic DNA sensing in cellular senescence has been recently reported[17–19]. We also observed that TBK1 was robustly activated following chemically induced DNA

Fig. 4 | AKT1 phosphorylates TBK1 at S510 to impede the STING signalosome. a, Key components of cGAS–STING signalling were examined by immunoblotting utilizing an antibody recognizing the phospho-AKT substrate. TBK1—but not cGAS, STING or TRAF3/6—was robustly modified by endogenous AKT and further enhanced by ectopic AKT1 expression. **b**, In vivo phospho-TBK1(AKT) was visualized by anti-FLAG immunoprecipitation enrichment of lysates from HCT116 cells harbouring FLAG-tagged TBK1 knock-in at the C terminus of endogenous TBK1, followed by immunoblotting using the phospho-AKT1 substrate antibody. **c**, The phospho-TBK1(AKT) signal disappeared in the presence of MK2206. **d**, The phospho-TBK1(AKT) signal was absent when TBK1 was expressed in AKT1-knockout HEK293 cells. An in vitro kinase assay with separately expressed and purified TBK1 and AKT1 revealed a direct modification of TBK1 by AKT1, which was prevented by MK2206. **e**, Mass spectrometry analysis showed that multiple phosphorylatable residues of TBK1 were directly or indirectly altered by AKT1. In particular, the level of phospho-S510 was greatly increased, whereas the phosphorylation levels of the proximal residues were substantially decreased. *, the residues richly phosphorylated and their phosphorylation is obviously altered; CCD, coiled-coil domain; PRM, phosphorylation-rich motif. **f**, Immunoblotting with the phospho-AKT substrate antibody failed to recognize TBK1 mutants in which the S510 residue was mutated (S510A and S510D). **g**, TBK1 activation was dramatically boosted when AKT1-mediated phosphorylation was prevented/impeded by point mutations and vice versa, as shown by immunoblots of phospho-S172 or total TBK1 with Phos-Tag or regular SDS–PAGE. **h**, The STING–TBK1 interaction was attenuated when TBK1 was mutated to mimic constitutive AKT1-induced phosphorylation (that is, elevated phosphorylation at S510 and dephosphorylation of proximal residues). **i**, The HER2 ICD disrupted the STING–TBK1 association in a dose-dependent manner. **j,k**, Following cGAMP stimulation, markedly enhanced activation of endogenous TBK1 and IRF3 was observed in TBK1 S510A knock-in DLD1 cells, which prevented AKT1-mediated phosphorylation (**j**) along with more intense STING aggregation and a better overlap with the Golgi marker GM130 (**k**). C1 and C2, clone 1 and clone 2, respectively, of knock-in DLD1 cells. Scale bars, 20 μm. $n = 3$ independent experiments for all panels. The unprocessed images of the blots are shown in Supplementary Fig. 8. The statistics source data are provided in Supplementary Table 1.
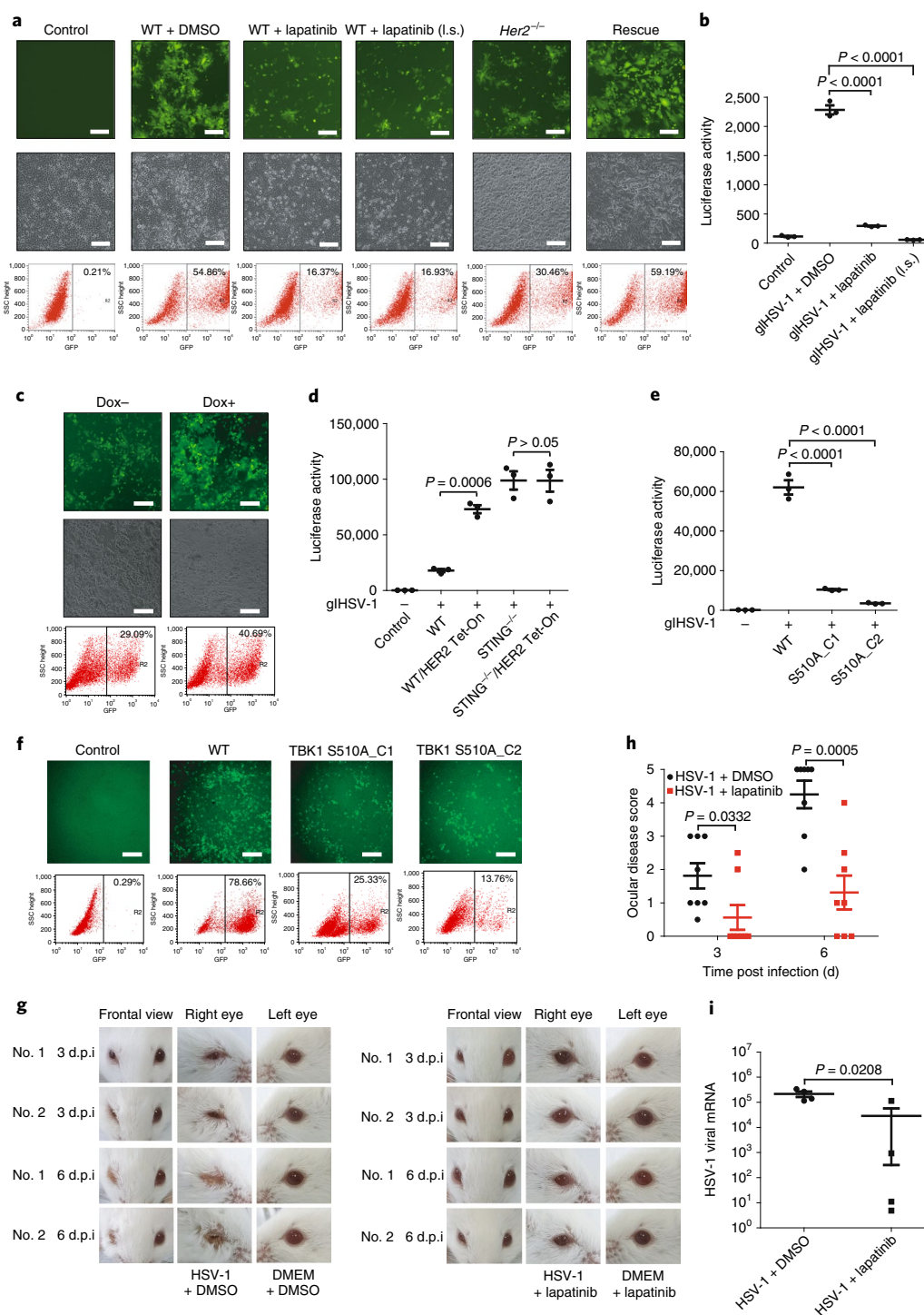
Fig. 5 | HER2 inhibits the antiviral defence initiated by cytosolic DNA sensing. a,b, Cellular resistance to GFP-tagged HSV-1 was assessed by microscopy (**a**, top and middle) and FACS (**a**, bottom) of NMuMG cells with replicating virus (GFP⁺) or by luciferase that had been integrated into the HSV-1 viral genome (**b**), both of which showed enhanced cellular viral resistance following lapatinib treatment or when *Her2* was genetically deleted. glHSV-, GFP and luciferase double-tagged HSV-1. **c,** Induced HER2 expression weakened the antiviral defence in DLD1 cells, as indicated by the increasing number of cells with replicating virus visualized by microscopy (top) and FACS (bottom). **d,** The effect of HER2 on HSV-1-infection potentiation disappeared following the genetic deletion of STING in DLD1 cells. **e,f,** Markedly enhanced antiviral defence was observed following HSV-1 infection in TBK1 S510A knock-in DLD1 cells, which prevented the AKT1-mediated modification, as revealed by luciferase (**e**) or microscopy (**f**, top) and FACS (**f**, bottom) of cells with replicating virus (GFP⁺). **g,h,** Corneal HSV-1 infection was performed on BALB/c mice and the scale of mouse ocular disease—eyelid swelling, shutting and crusting (shown by the representative images in **g**)—was assessed by disease scoring (**h**), which revealed a severe ocular infection of the mice caused by HSV-1 that was largely stopped by the ocular administration of lapatinib. The mean ± s.e.m. is shown for *n* = 8 mice per group. **i,** Quantitative PCR with reverse transcription (RT–qPCR) was performed to detect HSV-1 mRNA in the eyeballs of the killed mice at 6 days post infection (d.p.i.), which revealed markedly lower levels of viral loads in mice treated with lapatinib. The mean ± s.e.m. is shown for *n* = 4 mice per group. Unless otherwise specified, *n* = 3 independent experiments. *P* values are indicated; ANOVA test with Bonferroni correction. The statistics source data are provided in Supplementary Table 1. Scale bars, 100 μm.
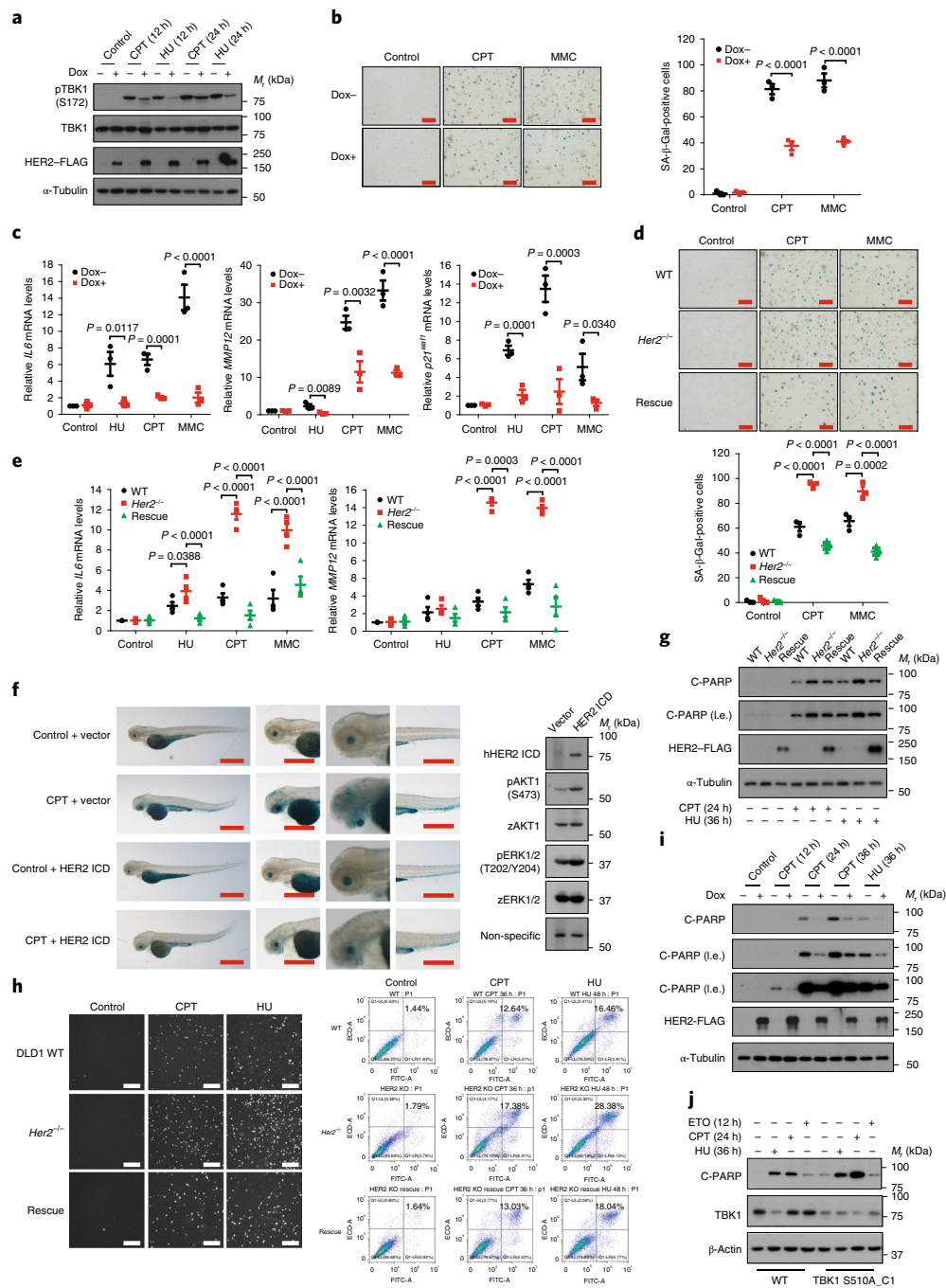
Fig. 6 | HER2 prevents damage-induced cellular senescence and apoptosis. a, DNA damage induced by CPT and HU led to the robust activation of endogenous TBK1, which was dampened by HER2 induction in DLD1 cells. **b,c**, The damage-induced cellular senescence of DLD1 cells was assessed by SA-β-Gal staining (**b**) and the mRNA expression levels (**c**) of the SASPs *IL6* (left) and *MMP12* (middle), and of *p21^waf1^* (right), which revealed that HER2 expression substantially alleviated the senescence of DLD1 cells in response to cellular damage. **d,e**, HER2 ablation in DLD1 cells led to an increase in senescence indicators, as demonstrated by SA-β-Gal staining (**d**) and the SASP expression levels in DLD1 cells (**e**). The reintroduction of HER2 through viral-vector-mediated delivery reversed these phenotypes. **f**, Cellular senescence was assessed in zebrafish embryos ($n = 30$) subjected to chemical-induced damage by incubation with CPT (50 nM). A strong phenotype of cellular senescence was detected in the heads and tails of zebrafish using SA-β-Gal staining (left); this could be prevented by ectopic expression of the ICD of human HER2 delivered by mRNA micro-injection at the one-cell stage of the zebrafish embryo and activated the downstream AKT and ERK MAPK signalling (right). **g,h**, Cellular damage induced by CPT and HU resulted in the robust production of cleaved PARPs (**g**)—an indicator of apoptosis—and phenotypes for apoptotic cells as indicated by propidium iodide staining (**h**, left) and FACS (**h**, right). Genetic ablation of *Her2* in DLD1 cells sensitized this damage-induced apoptosis, as detected by an increase in the levels of cleaved PARP (**g**) and apoptotic cell numbers (**h**); these phenotypes were rescued by the reintroduction of HER2 expression. **i**, Induced HER2 expression prevented the DNA-damage-induced apoptosis of DLD1 cells, as revealed by reduced levels of cleaved PARP. **j**, TBK1 S510A knock-in DLD1 cells were more sensitive following DNA damage and resulted in increased levels of cleaved PARP. $n = 3$ independent experiments for all panels; the mean ± s.e.m. is shown. *P* values are indicated; ANOVA test with Bonferroni correction. The unprocessed images of the blots are shown in Supplementary Fig. 8. The statistics source data are provided in Supplementary Table 1. Scale bars, 100 (**b,d,h**) and 500 μm (**f**). SA-β-Gal, senescence-associated β-galactosidase.

damage (Figs. 1k and 6a) and was at least partially dependent on STING signalling (Supplementary Fig. 6a). HER2 expression markedly inhibited the damage-induced TBK1 activation, indicating a critical role for HER2 in the regulation of DNA sensing during the cellular-damage response (Fig. 6a). HER2 induction itself did not promote cellular senescence; in contrast, it effectively prevented the damage-induced senescence phenotype, as revealed by senescence-associated β-galactosidase (SA-β-Gal) staining (Fig. 6b) and senescence-associated secretory phenotypes (SASPs; Fig. 6c), fully dependent on STING signalling (Supplementary Fig. 6b,c). In contrast, HER2 ablation exaggerated this damage-induced cellular senescence, which was alleviated by HER2 reconstitution (Fig. 6d,e), suggesting that HER2 is responsible for the regulation of damage-induced senescence.

We also examined this particular role for HER2 on senescence at the whole-animal level using the zebrafish model[51]. Incubation of zebrafish embryos with the DNA-damage inducer camptothecin (CPT) resulted in a strong senescence phenotype, as demonstrated by the increased number of SA-β-Gal-positive cells in the head and tail of the zebrafish (Fig. 6f). Human HER2 or its ICD interacted with zebrafish STING and suppressed the activation of zebrafish TBK1 (Supplementary Fig. 6d–f). Ectopic expression of the human HER2 ICD in zebrafish embryos substantially reduced the level of senescent cells in response to damage (Fig. 6f). These observations suggest that HER2 regulates damage-induced cellular senescence by governing cytosolic DNA sensing.

Cytosolic DNA sensing through STING also leads to a strong apoptosis response[52]. Apoptosis of DLD1 cells following cellular damage was revealed by measuring cleaved poly (ADP-ribose) polymerases (PARPs) and propidium iodide staining of apoptotic cells via fluorescence-activated cell sorting (FACS; Fig. 6g,h). Damage-induced apoptosis was significantly sensitized in *Her2*$^{-/-}$ cells, which was rescued by HER2 reconstitution (Fig. 6g,h). In contrast, induced expression of HER2 alleviated the apoptotic phenotypes (Fig. 6i and Supplementary Fig. 6g), and the effect of HER2 was fully dependent on STING signalling (Supplementary Fig. 6h). In addition, by preventing AKT1-mediated TBK1 phosphorylation, DLD1 cells with TBK1 S510A knock-in mutagenesis were more vulnerable to damage-induced apoptosis (Fig. 6j). These consistent observations suggest that the HER2–AKT1 axis prevents apoptosis induced by cellular damage by suppressing cytosolic DNA damage.

HER2 protects cancer cells from STING-mediated antitumour immunity. Aberrant DNA fragments are ubiquitous in various cancer cells and monitored by cytosolic DNA sensing occurring in both immune and cancer cells[20]. Because of previous observations of enhanced ISG expression and lymphoid cell infiltration following HER2 inhibition strategies in tumour therapy[38–42], we focused on the effects of HER2 expression. Using a naturally occurring and constitutively active STING SAVI mutant (R281Q)[53,54], we generated a cell system with inducible but constitutive STING signalling, in comparison with the inducible wild-type STING in its resting state (Fig. 7a). The expression of STING R281Q in B16 cells alone induced cellular senescence, which was sensitized following stimulation by cellular damage but was alleviated by HER2 expression (Fig. 7b and Supplementary Fig. 7a–c). B16-F10 cells were subcutaneously implanted into wild-type C57BL/6 mice and melanomas harbouring the STING R281Q had very poor xenograft growth (Fig. 7c and Supplementary Fig. 7d), whereas the administration of a neutralizing antibody targeting IFNAR1 restored this growth arrest (Fig. 7d), suggesting a critical role of type I IFNs in this antitumour model. As expected, we observed a massive increase in the infiltration of immune cells, including CD4$^+$ and CD8$^+$ T cells, into melanomas expressing constitutively active STING (Fig. 7e and Supplementary Fig. 7e,f), indicating increased antitumour immunity following the activation of STING signalling. In contrast, HER2 induction

reduced the infiltration of immune cells in melanomas (Fig. 7e and Supplementary Fig. 7f) and significantly increased the tumour volume (Fig. 7c,d and Supplementary Fig. 7d) to levels comparable to those observed when the IFN-I pathway was blocked. These observations suggest that HER2 alleviates STING-mediated antitumour immunity by suppressing cytosolic DNA sensing.

Discussion

Cytosolic DNA sensing is a key innate mechanism of most cells for the recognition of cellular damage and abnormalities. In addition to its role in IFN and cytokine production, the cGAS–STING pathway frequently leads to cellular senescence[17–19] and cell death, and boosts antitumour immunity in a tumour setting[20–22]. Because abnormal DNA patterns are a major feature of cancer cells, elucidating how these cells evade damage surveillance is an important topic for understanding tumorigenesis. In particular, it remains unclear how classic oncogenic pathways are involved in these innate immune mechanisms. In this report, we show HER2, a well-defined RTK that is frequently amplified and activated in multiple cancers, is a natural and potent suppressor of cytosolic DNA sensing. We demonstrate that HER2 is vital to effective suppression of cGAS–STING signalling and prevention of cancer cells from entering cellular senescence, undergoing apoptosis and responding to antitumour immunity (Fig. 7f). Interestingly, EGFR and other ERBB-family RTKs are incapable of such suppression in the diverse primary and culture cells that we examined. Unlike HER2, EGFR is unable to physically associate with STING, although a recent report indicated that EGFR is involved in cytosolic RNA sensing[55]. Similarly, EGFR-induced mild activation of cGAS–STING signalling in the absence or presence of HER2 and AKT1 suggests that the EGFR–HER2 heterodimer does not participate in STING regulation. The HER2–STING interaction mostly occurs in ER compartments and partially at the Golgi apparatus, thus differing from the HER2 heterodimer, which is mostly found at the cell plasma membrane[56].

The overwhelming observations of HER2 amplification or hyperactivation in metastatic breast, prostate, lung and ovarian cancers indicate that HER2 is a key oncogene in tumorigenesis[36,37]. At present, the mechanistic insights into HER2-induced transformation and tumorigenesis focus mainly on its effects on hyperproliferation and apoptosis prevention[37]. However, some investigations have suggested roles for HER2 in blocking antitumour immunity[38–40,42,57] and PTEN-loss-induced cellular senescence[57] despite the lack of detailed mechanisms. Our current data from molecular and physiological observations illustrate an essential role of HER2 in blocking cytosolic DNA sensing. The integration of HER2 into the cellular-damage surveillance system adds an interesting dimension to the function of HER2 and links HER2 to cellular senescence, apoptosis, antitumour immunity and antiviral immunity, where the cGAS–STING-mediated sensing of cytosolic DNA plays a substantial role[5,58]. HER2 may also contribute to the regulation of autophagy and metabolism, in which STING and TBK1/IKKε are closely involved[29,59–61]. This additional layer of protection could be an adaptive mechanism to avoid excessive reactions leading to potential autoimmune damage owing to the exposure of native nucleic acids[15,16]. Notably, the HER2–AKT1 axis is robustly activated and subcellular localization of HER2 is markedly redistributed during cytosolic DNA sensing, which may involve TBK1 activity[62,63], but this mechanism requires further elucidation.

Pathogenic DNA is sensed in the cytoplasm mainly by cGAS[2], which results in the synthesis of the small messenger molecule cGAMP. The binding of cGAMP[1,64] drives STING to translocate from the ER to the Golgi apparatus and perinuclear microsome through an as yet undefined mechanism. Meanwhile, the STING signalosome is assembled and IRF3 is activated by the kinase TBK1 during STING translocation[10–12,18,65] by a process that is still poorly understood. We observed the rapid STING aggregation
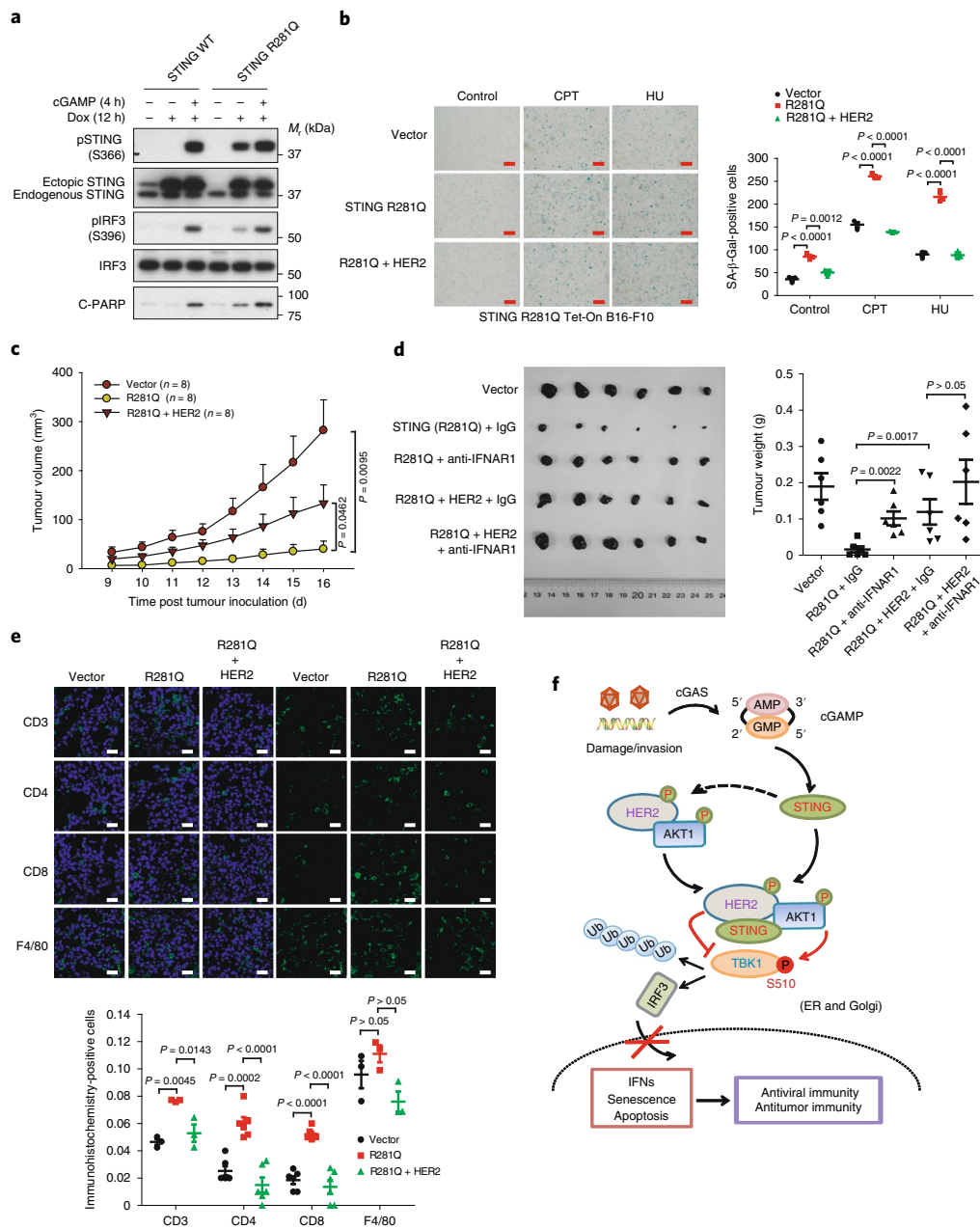
Fig. 7 | HER2 protects cancer cells from STING-mediated antitumour immunity. a, The STING SAVI mutant R281Q was constitutively active and DLD1 cells stably expressing this mutant showed a milder yet robust activity, as indicated by phospho-STING(S366), the activation of endogenous IRF3 and the induced apoptosis measured by cleaved PARPs. **b**, The expression of STING R281Q and CPT- or HU-induced cellular damage resulted in cellular senescence in B16-F10 melanoma cells, which was alleviated by the induction of HER2 expression (left). The statistics of cells that stained for SA-β-Gal were calculated (right). **c**, Xenograft growth of B16-F10 cells implanted subcutaneously into wild-type C57BL/6 mice revealed a marked decrease in the growth of melanoma cells expressing the STING SAVI mutant. HER2 expression partially rescued this phenotype. The mean ± s.e.m. measured from 9 d post tumour inoculation is shown for $n = 8$ inoculations per group. **d**, Administration of a neutralizing antibody against IFNAR1 partially reversed the decrease in tumour growth induced by the STING SAVI mutant, comparable with melanoma cells ectopically expressing HER2 (left; $n = 6$). The statistics of the tumour weights were calculated. The mean ± s.e.m. measured at 16 d post tumour inoculation for $n = 6$ inoculations per group is shown. **e**, A robust increase in the number of infiltrating immune cells in melanomas, particularly CD4+ and CD8+ T cells, was detected by fluorescent immunohistochemistry following the expression of the STING SAVI mutant. HER2 expression significantly reduced the infiltration of immune cells, including CD4+ and CD8+ T cells, in B16 melanomas (top). The statistics for the immunohistochemistry-positive cells were calculated (bottom) from the counts from three or six sections. **f**, Cytosolic sensing of DNA not only leads to cGAMP production and the assembly of the STING signalosome but also activates the HER2–AKT1 axis, which is recruited by STING and modifies TBK1 directly at the S510 residue to impede the assembly of the STING signalosome. HER2-mediated suppression of cytosolic DNA sensing is crucial to prevent cells from exacerbating their damage, suppress danger responses to the production of IFNs, senescence or apoptosis and, in the tumour setting, to enhance the tolerance of tumour cells to antitumour immunity. Unless otherwise specified, $n = 3$ independent experiments; the mean ± s.e.m. is shown. *P* values are indicated; ANOVA test with Bonferroni correction. The unprocessed images of the blots are shown in Supplementary Fig. 8. The statistics source data are provided in Supplementary Table 1. Scale bars, 100 (**b**) and 20 µm (**e**).

and translocation to the Golgi apparatus following cGAMP stimulation, which is critically regulated by the expression levels and activation of HER2. Our findings show that the HER2 ICD binds to the C-terminal domain of STING, which occurs mostly in the ER compartments. We observed that the binding of HER2 to STING leads to a marked dissociation between STING and TBK1 as well as a strongly compromised TBK1 K63-linked ubiquitination, a step known to be critical for TBK1 activation[46–49]. We also observed the intriguing recruitment of AKT1 to STING by HER2 and the AKT1-induced alteration of a myriad of phosphorylatable residues on TBK1. According to a recently proposed model, these residues are located at an interface possibly for inter-homodimer interactions in a higher-order of TBK1 assembly[28]. Recruitment of AKT1 for the direct modification of TBK1 is the most plausible mechanism for the potent inhibition induced by HER2, although other complementary mechanisms cannot be fully excluded. We illustrate the critical role of this suppressive phosphorylation in cellular damage response and antiviral immunity using a CRISPR-based strategy to prevent this specific modification. A previous report showed the AKT1-mediated phosphorylation of cGAS[66]; however, in contrast to the robust signal of AKT1-mediated TBK1 phosphorylation, we failed to detect this modification in our setting. The specificity of AKT1 among other AKT-family members is also intriguing, although distinct expression patterns and phenotypes of individual AKT knockout have been reported[67,68]. We have observed that only AKT1 can be effectively recruited to STING by HER2 and only AKT1 effectively phosphorylates TBK1 in cells, thus demonstrating their specificity in regulating cGAS–STING signalling.

In conclusion, our model indicates that the levels and activity of HER2 serve as a determinant to control the magnitude of the innate immune sensing of cellular damage and microbial invasion, thus governing the relevant phenotypic responses. Consistent with this idea, our research suggests that the pharmacological targeting of HER2 or AKT1, by enhancing cytosolic DNA sensing, offers potential therapeutic benefits for antiviral defence and antitumour immunity.

Online content

Any methods, additional references, Nature Research reporting summaries, source data, statements of code and data availability and associated accession codes are available at https://doi.org/10.1038/s41556-019-0352-z.

References

1. Gao, P. et al. Cyclic [G(2′,5′)pA(3′,5′)p] is the metazoan second messenger produced by DNA-activated cyclic GMP-AMP synthase. *Cell* **153**, 1094–1107 (2013).
2. Sun, L., Wu, J., Du, F., Chen, X. & Chen, Z. J. Cyclic GMP-AMP synthase is a cytosolic DNA sensor that activates the type I interferon pathway. *Science* **339**, 786–791 (2013).
3. Chen, Q., Sun, L. & Chen, Z. J. Regulation and function of the cGAS–STING pathway of cytosolic DNA sensing. *Nat. Immunol.* **17**, 1142–1149 (2016).
4. Takeuchi, O. & Akira, S. Pattern recognition receptors and inflammation. *Cell* **140**, 805–820 (2010).
5. Roers, A., Hiller, B. & Hornung, V. Recognition of endogenous nucleic acids by the innate immune system. *Immunity* **44**, 739–754 (2016).
6. Ishikawa, H. & Barber, G. N. STING is an endoplasmic reticulum adaptor that facilitates innate immune signalling. *Nature* **455**, 674–678 (2008).
7. Zhong, B. et al. The adaptor protein MITA links virus-sensing receptors to IRF3 transcription factor activation. *Immunity* **29**, 538–550 (2008).
8. Sun, W. et al. ERIS, an endoplasmic reticulum IFN stimulator, activates innate immune signaling through dimerization. *Proc. Natl Acad. Sci. USA* **106**, 8653–8658 (2009).
9. Moretti, J. et al. STING senses microbial viability to orchestrate stress-mediated autophagy of the endoplasmic reticulum. *Cell* **171**, 809–823.e813 (2017).
10. Luo, W. W. et al. iRhom2 is essential for innate immunity to DNA viruses by mediating trafficking and stability of the adaptor STING. *Nat. Immunol.* **17**, 1057–1066 (2016).
11. Saitoh, T. et al. Atg9a controls dsDNA-driven dynamic translocation of STING and the innate immune response. *Proc. Natl Acad. Sci. USA* **106**, 20842–20846 (2009).
12. Dobbs, N. et al. STING activation by translocation from the ER is associated with infection and autoinflammatory disease. *Cell Host Microbe* **18**, 157–168 (2015).
13. Sharma, S. et al. Triggering the interferon antiviral response through an IKK-related pathway. *Science* **300**, 1148–1151 (2003).
14. Fitzgerald, K. A. et al. IKKe and TBK1 are essential components of the IRF3 signaling pathway. *Nat. Immunol.* **4**, 491–496 (2003).
15. Gao, D. et al. Activation of cyclic GMP-AMP synthase by self-DNA causes autoimmune diseases. *Proc. Natl Acad. Sci. USA* **112**, E5699–E5705 (2015).
16. Crampton, S. P. & Bolland, S. Spontaneous activation of RNA-sensing pathways in autoimmune disease. *Curr. Opin. Immunol.* **25**, 712–719 (2013).
17. Dou, Z. et al. Cytoplasmic chromatin triggers inflammation in senescence and cancer. *Nature* **550**, 402–406 (2017).
18. Yang, H., Wang, H., Ren, J., Chen, Q. & Chen, Z. J. cGAS is essential for cellular senescence. *Proc. Natl Acad. Sci. USA* **114**, E4612–E4620 (2017).
19. Gluck, S. et al. Innate immune sensing of cytosolic chromatin fragments through cGAS promotes senescence. *Nat. Cell Biol.* **19**, 1061–1070 (2017).
20. Fu, J. et al. STING agonist formulated cancer vaccines can cure established tumors resistant to PD-1 blockade. *Sci. Transl. Med.* **7**, 283ra252 (2015).
21. Demaria, O. et al. STING activation of tumor endothelial cells initiates spontaneous and therapeutic antitumor immunity. *Proc. Natl Acad. Sci. USA* **112**, 15408–15413 (2015).
22. Deng, L. et al. STING-dependent cytosolic DNA sensing promotes radiation-induced type I interferon-dependent antitumor immunity in immunogenic tumors. *Immunity* **41**, 843–852 (2014).
23. Bakhoum, S. F. et al. Chromosomal instability drives metastasis through a cytosolic DNA response. *Nature* **553**, 467–472 (2018).
24. Mackenzie, K. J. et al. cGAS surveillance of micronuclei links genome instability to innate immunity. *Nature* **548**, 461–465 (2017).
25. Tang, C. H. et al. Agonist-mediated activation of STING induces apoptosis in malignant B cells. *Cancer Res.* **76**, 2137–2152 (2016).
26. Corrales, L. et al. Direct activation of STING in the tumor microenvironment leads to potent and systemic tumor regression and immunity. *Cell Rep.* **11**, 1018–1030 (2015).
27. Liu, S. et al. Phosphorylation of innate immune adaptor proteins MAVS, STING, and TRIF induces IRF3 activation. *Science* **347**, aaa2630 (2015).
28. Zhang, C. et al. Structural basis of STING binding with and phosphorylation by TBK1. *Nature* **567**, 394–398 (2019).
29. Wild, P. et al. Phosphorylation of the autophagy receptor optineurin restricts *Salmonella* growth. *Science* **333**, 228–233 (2011).
30. Hou, F. et al. MAVS forms functional prion-like aggregates to activate and propagate antiviral innate immune response. *Cell* **146**, 448–461 (2011).
31. Porritt, R. A. & Hertzog, P. J. Dynamic control of type I IFN signalling by an integrated network of negative regulators. *Trends Immunol.* **36**, 150–160 (2015).
32. Liu, J., Qian, C. & Cao, X. Post-translational modification control of innate immunity. *Immunity* **45**, 15–30 (2016).
33. Zhang, Q. et al. Hippo signalling governs cytosolic nucleic acid sensing through YAP/TAZ-mediated TBK1 blockade. *Nat. Cell Biol.* **19**, 362–374 (2017).
34. Xiang, W. et al. PPM1A silences cytosolic RNA sensing and antiviral defense through direct dephosphorylation of MAVS and TBK1. *Sci. Adv.* **2**, e1501889 (2016).
35. Liu, S. et al. Lck/Hck/Fgr-Mediated Tyrosine Phosphorylation Negatively Regulates TBK1 to Restrain Innate Antiviral Responses. *Cell Host Microbe* **21**, 754–768.e755 (2017).
36. Moasser, M. M. The oncogene HER2: its signaling and transforming functions and its role in human cancer pathogenesis. *Oncogene* **26**, 6469–6487 (2007).
37. Arteaga, C. L. & Engelman, J. A. ERBB receptors: from oncogene discovery to basic science to mechanism-based cancer therapeutics. *Cancer Cell* **25**, 282–303 (2014).
38. Gennari, R. et al. Pilot study of the mechanism of action of preoperative trastuzumab in patients with primary operable breast tumors overexpressing HER2. *Clin. Cancer Res.* **10**, 5650–5655 (2004).
39. Kroemer, G., Senovilla, L., Galluzzi, L., Andre, F. & Zitvogel, L. Natural and therapy-induced immunosurveillance in breast cancer. *Nat. Med.* **21**, 1128–1138 (2015).
40. Sistigu, A. et al. Cancer cell-autonomous contribution of type I interferon signaling to the efficacy of chemotherapy. *Nat. Med.* **20**, 1301–1309 (2014).
41. Park, S. et al. The therapeutic effect of anti-HER2/neu antibody depends on both innate and adaptive immunity. *Cancer Cell* **18**, 160–170 (2010).

42. Stagg, J. et al. Anti-ErbB-2 mAb therapy requires type I and II interferons and synergizes with anti-PD-1 or anti-CD137 mAb therapy. *Proc. Natl Acad. Sci. USA* **108**, 7142–7147 (2011).

43. Fang, R. et al. MAVS activates TBK1 and IKKepsilon through TRAFs in NEMO dependent and independent manner. *PLoS Pathog.* **13**, e1006720 (2017).

44. Liu, S. et al. MAVS recruits multiple ubiquitin E3 ligases to activate antiviral signaling cascades. *eLife* **2**, e00785 (2013).

45. Song, G. et al. E3 ubiquitin ligase RNF128 promotes innate antiviral immunity through K63-linked ubiquitination of TBK1. *Nat. Immunol.* **17**, 1342–1351 (2016).

46. Tu, D. et al. Structure and ubiquitination-dependent activation of TANK-binding kinase 1. *Cell Rep.* **3**, 747–758 (2013).

47. Shu, C. et al. Structural insights into the functions of TBK1 in innate antimicrobial immunity. *Structure* **21**, 1137–1148 (2013).

48. Larabi, A. et al. Crystal structure and mechanism of activation of TANK-binding kinase 1. *Cell Rep.* **3**, 734–746 (2013).

49. Li, S., Wang, L., Berman, M., Kong, Y. Y. & Dorf, M. E. Mapping a dynamic innate immunity protein interaction network regulating type I interferon production. *Immunity* **35**, 426–440 (2011).

50. Jaishankar, D., et al. An off-target effect of BX795 blocks herpes simplex virus type 1 infection of the eye. *Sci. Transl. Med.* **10**, eaan5861 (2018).

51. Kishi, S. et al. The identification of zebrafish mutants showing alterations in senescence-associated biomarkers. *PLoS Genet.* **4**, e1000152 (2008).

52. Gulen, M. F. et al. Signalling strength determines proapoptotic functions of STING. *Nat. Commun.* **8**, 427 (2017).

53. Liu, Y. et al. Activated STING in a vascular and pulmonary syndrome. *N. Engl. J. Med.* **371**, 507–518 (2014).

54. Melki, I. et al. Disease-associated mutations identify a novel region in human STING necessary for the control of type I interferon signaling. *J. Allergy Clin. Immunol.* **140**, 543–552 (2017).

55. Ueki, I. F. et al. Respiratory virus-induced EGFR activation suppresses IRF1-dependent interferon λ and antiviral defense in airway epithelium. *J. Exp. Med.* **210**, 1929–1936 (2013).

56. Cho, H. S. et al. Structure of the extracellular region of HER2 alone and in complex with the Herceptin Fab. *Nature* **421**, 756–760 (2003).

57. Ahmad, I. et al. HER2 overcomes PTEN (loss)-induced senescence to cause aggressive prostate cancer. *Proc. Natl Acad. Sci. USA* **108**, 16392–16397 (2011).

58. Li, T. & Chen, Z. J. The cGAS-cGAMP-STING pathway connects DNA damage to inflammation, senescence, and cancer. *J. Exp. Med.* **215**, 1287–1299 (2018).

59. Zhao, P. et al. TBK1 at the crossroads of inflammation and energy homeostasis in adipose tissue. *Cell* **172**, 731–743 (2018).

60. Pilli, M. et al. TBK-1 promotes autophagy-mediated antimicrobial defense by controlling autophagosome maturation. *Immunity* **37**, 223–234 (2012).

61. Gui, X. et al. Autophagy induction via STING trafficking is a primordial function of the cGAS pathway. *Nature* **567**, 262–266 (2019).

62. Ou, Y. H. et al. TBK1 directly engages Akt/PKB survival signaling to support oncogenic transformation. *Mol. Cell* **41**, 458–470 (2011).

63. Xie, X. et al. IκB kinase ε and TANK-binding kinase 1 activate AKT by direct phosphorylation. *Proc. Natl Acad. Sci. USA* **108**, 6474–6479 (2011).

64. Li, X. D. et al. Pivotal roles of cGAS-cGAMP signaling in antiviral defense and immune adjuvant effects. *Science* **341**, 1390–1394 (2013).

65. Ishikawa, H., Ma, Z. & Barber, G. N. STING regulates intracellular DNA-mediated, type I interferon-dependent innate immunity. *Nature* **461**, 788–792 (2009).

66. Seo, G. J. et al. Akt kinase-mediated checkpoint of cGAS DNA sensing pathway. *Cell Rep.* **13**, 440–449 (2015).

67. Cho, H. et al. Insulin resistance and a diabetes mellitus-like syndrome in mice lacking the protein kinase Akt2 (PKBβ). *Science* **292**, 1728–1731 (2001).

68. Chen, W. S. et al. Growth retardation and increased apoptosis in mice with homozygous disruption of the *akt1* gene. *Genes Dev.* **15**, 2203–2208 (2001).

Author contributions

S.W., Q.Z. and F.Z. carried out most of the experiments. F.M., S.L., R.Z. and Q.W. contributed to several experiments. X.L., L.S., J.H., J.Q., Z.X., S.O., H.S., X.-H.F. and J.Z. helped with the data analyses and were involved in discussions of the data. P.X. conceived the study and experimental design and wrote the manuscript.

Competing interests

The authors declare no competing interests.

Additional information

Supplementary information is available for this paper at https://doi.org/10.1038/s41556-019-0352-z.

Reprints and permissions information is available at www.nature.com/reprints.

Correspondence and requests for materials should be addressed to P.X.

Publisher's note: Springer Nature remains neutral with regard to jurisdictional claims in published maps and institutional affiliations.

Methods

Expression plasmids, viruses, reagents and antibodies. Expression plasmids encoding FLAG-, Myc- or haemagglutinin (HA)-tagged wild-type, mutant or truncated human TBK1, IRF3, RIG-I, MAVS, cGAS, STING, ubiquitin and LCK in addition to reporters of IFNβ_Luc and 5×ISRE_Luc have been described previously[33,35]. The open reading frames (ORFs) or truncations of *Her2*, *Akt1* and *TRAF3/6* were obtained from the Invitrogen ORF lite clone collection cDNA library by PCR and constructed using the pRK5 mammalian expression vector with the indicated tags. Site-directed mutagenesis to generate expression plasmids encoding HER2 K753M and TBK1 S499D, S510A/D, 3TS/A (T514A + T517A + S518A), 3TS/A + S510D, R507A, L505R and S499A + S510D were performed using a kit from Stratagene. All coding sequences were verified by DNA sequencing and detailed information of plasmids is provided in the attached Supplementary Table 2 and on request.

The GFP and luciferase double-tagged HSV-1 was a gift from J. Han (Xiamen University). HSV-1 (strain COS) and VacV were provided by Z. Jiang (Peking University). The pharmacological reagents U0126 (Selleck), MK2206 (Selleck), ARRY-380 (Selleck), WZ4002 (Selleck), icotinib (Selleck), lapatinib (water soluble and lipid soluble; Selleck), doxycycline (Sangon Biotech), 2′3′-cGAMP (Invivogen), poly(dA:dT) (Invivogen), puromycin (Yesen), G418 (Yesen), CPT (Sigma), HU (Sigma), mitomycin C (Sigma), EGF (R&D Systems) and NRG1-β1 (PeproTech) were purchased and used according to the manufacturer's instructions.

Detailed information on all of the antibodies applied in immunoblotting, immunoprecipitation, immunofluorescence and neutralization are provided in Supplementary Table 3. The monoclonal anti-IRF3 (4302S; 1:2,000 dilution), anti-pIRF3(S396) (4947S; 1:5,000 dilution), anti-TBK1 (3504S; 1:5,000 dilution), anti-pTBK1(S172) (5483S; 1:3,000 dilution), anti-STING (13647S; 1:1,000 dilution), anti-pSTING(S366) (85735S; 1:1,000 dilution), anti-HER2 (2165S; 1:1,000 dilution), anti-EGFR (4267S; 1:1,000 dilution), anti-pEGFR(Y845) (2231S; 1:1,000 dilution), anti-HER3 (4754S; 1:1,000 dilution), anti-pHER3(Y1289) (4791S; 1:1,000 dilution), anti-AKT1 (2938S; 1:1,000 dilution), anti-pAKT substrate (phospho-RXXS*/T*) (9614S; 1:1,000 dilution), anti-pAKT1(S473) (4060S; 1:1,000 dilution), anti-pAKT1(T308) (13038S; 1:1,000 dilution), anti-pPRAS40(T246) (2997S; 1:1,000 dilution), anti-PRAS40 (2691S; 1:1,000 dilution), anti-AKT2 (3063S; 1:1,000 dilution), anti-AKT3 (14982S; 1:1,000 dilution), anti-ERK1/2 (4695T; 1:1,000 dilution), anti-pERK1/2(T202 Y204) (4370T; 1:1,000 dilution), anti-pY100 (9411S; 1:2,000 dilution), anti-cleaved PARP (5625S; 1:1,000 dilution), anti-calnexin (2679S; 1:200 dilution), anti-Myc (2276S; 1:1,000 dilution) and anti-HA (3724S; 1:1,000 dilution) antibodies were purchased from Cell Signaling Technology. The anti-pIRF3(S386) (ab76493; 1:3,000 dilution), anti-CD3 (ab16669; 1:100 dilution), anti-STING (ab181125; 1:100 dilution) and anti-GM130 (52649; 1:200 dilution) antibodies were purchased from Abcam, and anti-α-tubulin (T6199-200UL; 1:10,000 dilution), anti-β-actin (A5441-100UL; 1:10,000 dilution), anti-HA (H9658; 1:200 dilution), anti-PDIA3 (AMAb90988; 1:2,000 dilution) and anti-FLAG (M2) (F3165-5MG; 1:5,000 dilution) antibodies were purchased from Sigma. The anti-CD4 (cat. no. 14976680; 1:100 dilution) and anti-CD8 (cat. no. 14080880, 1:100 dilution) antibodies were purchased from eBioscience. The anti-F4/80 antibody (MCA497RT; 1:100 dilution) was purchased from Bio-Rad. Anti-HER2 (3B5) (sc-33684; 1:100 dilution) was purchased from Santa Cruz Biotech. Anti-GM130 (cat. no. 610822; 1:2,000 dilution) was purchased from BD Bioscience. The anti-mouse IFNAR1 (clone MAR1-5A3; BE0241) and anti-mouse IgG1 (clone MOPC-21; BP0083) antibodies were purchased from Bio X Cell.

Cell culture, transfections and infections. NMuMG, HEK293, HCT116, DLD1, MEF and B16-F10 cells were obtained from the ATCC, and BT474 and SKBR-3 cells were obtained from Cell Bank (CAS Collection Committee). Peritoneal macrophages were obtained from C57BL/6 male mice at 6–8 weeks of age using the Brewer thioglycollate medium (Sigma)-induced approach, and human PBMCs were isolated from healthy human blood using a standard protocol. The care of animals used in experiments was in accordance with guidelines of and approved by the Laboratory Animal Committee of Zhejiang University. None of the cell lines used in this study were found in the database of commonly misidentified cell lines, which is maintained by ICLAC and NCBI Biosample. The cell lines were frequently checked for morphology under a microscope and tested for mycoplasma contamination but were not authenticated. All cell lines—except peritoneal macrophages and BT474, which were maintained in RPMI 1640 medium—were cultured in DMEM with 10% fetal bovine serum at 37 °C in 5% CO_2 (v/v). DLD1, NMuMG and MEF cells with inducible HER2 and STING expression were generated by transduction with a lentiviral vector containing the inducible Tet-On system followed by the ORF of HER2 and STING and were selected with the antibiotic G418 at a concentration of 1,500 µg ml^{-1} for one week. Lipofectamine 3000 (Invitrogen) or polyethylenimine (Polysciences) transfection reagents were used for the plasmid and poly(dA:dT) transfections. Infections with HSV-1 or VacV were performed as previously described[35]. Briefly, viruses at the indicated titre (multiplicity of infection of 0.5–5) were added into fresh and serum-free media, and the cells were incubated at 37 °C in 5% CO_2 (v/v) for 1 h with mild shaking every 15 min. The virus-containing medium was then replaced with fresh medium containing 10% fetal bovine serum.

Luciferase reporter assay. HEK293 cells were transfected with the indicated reporters (100 ng) bearing an ORF coding for the Firefly luciferase along with the pRL-Luc with the Renilla luciferase ORF as the internal control for transfection and other expression vectors specified in the results section. Briefly, at 12 h post transfection, the cells were treated with the indicated inhibitors and lysed in a passive lysis buffer (Promega) 24 h after transfection. The luciferase assays were performed using a dual luciferase assay kit (Promega), quantified with POLARstar Omega (BMG Labtech) and normalized to the internal Renilla-luciferase activity.

RT–qPCR assay. NMuMG, DLD1, B16-F10 and HCT116 cells stimulated with cGAMP, CPT, HU and mitomycin C were lysed and total RNA was extracted using an RNAeasy extraction kit (Axygen). Complimentary DNA was generated using a one-step iScript cDNA synthesis kit (Vazyme) and RT–qPCR was performed using EvaGreen qPCR master mixes (Abm) and a CFX96 real-time PCR system (Bio-Rad). Relative quantification was expressed as $2^{-\Delta Ct}$, where C_t is the difference between the main C_t value of the triplicates of the sample and the C_t value of endogenous *L19* mRNA. All of the human, mouse and virus primers used in the RT–qPCR assay are listed in Supplementary Table 4.

Coimmunoprecipitation and immunoblotting. HEK293 and DLD1 cells stimulated with cGAMP or transfected with the specified plasmids encoding Myc-, FLAG- or HA-tagged EGFR, HER2s, RIG-I, MAVS, cGAS, AKT1, AKT2, AKT3, TRAF3/6, TBK1s, IRF3s or STING were lysed in a modified Myc lysis buffer (MLB; 20 mM Tris–HCl, 200 mM NaCl, 10 mM NaF, 1 mM NaV_2O_4, 1% NP-40, 20 mM β-glycerophosphate and protease inhibitor, pH 7.5)[69]. The cell lysates were then subjected to immunoprecipitation using antibodies against FLAG (Sigma, F3165-5MG; 1:200 dilution), Myc (CST, 2276S; 1:200 dilution) or HA (Sigma, H9658; 1:200 dilution) for transfected proteins or using anti-HER2 (2165S; 1:100 dilution) antibody for endogenous proteins. After three or four washes with MLB, the adsorbed proteins were resolved by SDS–PAGE (Bio-Rad) and subjected to immunoblotting with the indicated antibodies. The cell lysates were included in these analyses to control for protein abundance.

In vitro kinase assay. Wild-type or AKT1-knockout HEK293 cells were transfected with the HA-tagged TBK1 plasmid or FLAG-tagged AKT1 in the absence or presence of MK2206 (10 µM). The cells were lysed in modified MLB lysis buffer 24 h after transfection. Immunoprecipitation was performed using anti-FLAG (Sigma, F3165-5MG; 1:200 dilution) or anti-HA (Sigma, H9658; 1:200 dilution) antibodies. After four washes in MLB and one wash in kinase assay buffer (20 µM ATP, 20 mM Tris–HCl, 1 mM EGTA, 5 mM $MgCl_2$, 0.02% 2-mercapto-ethanol, 0.03% Brij-35 and 0.2 mg ml^{-1} BSA, pH 7.4), the immunoprecipitated HA-tagged TBK1 and FLAG-tagged AKT1 were incubated in the kinase assay buffer at 30 °C for 60 min on a THERMO-SHAKER. The reaction was stopped by the addition of 2×SDS loading buffer, and the samples were subjected to SDS–PAGE and specified immunoblotting.

Immunofluorescence, microscopy and FACS. To visualize the subcellular localization of the transfected or induced STING and HER2, BT474 or DLD1 cells expressing the inducible proteins specified in the Results section (including FLAG-tagged HER2 or HA or FLAG-tagged STING for 24 h) were treated with either cGAMP or lapatinib for the indicated times, fixed in 4% paraformaldehyde, blocked in 2% BSA in PBS for 1 h, and incubated sequentially with primary antibodies—anti-HA (CST, 3724S, 1:200 dilution), anti-FLAG (M2; Sigma, F3165; 1:300 dilution), anti-STING (Abcam, ab181125; 1:100 dilution), anti-HER2 (3B5) (Santa Cruz Biotech, sc-33684; 1:100 dilution), anti-HER2 (Cell Signaling Technology, 2165S; 1:100 dilution), anti-PDIA3 (Sigma, AMAb90988; 1:2,000 dilution), anti-calnexin (Cell Signaling Technology, 2679S; 1:200 dilution), anti-GM130 (BD Bioscience, ab610822; 1: 2,000 dilution) or anti-GM130 (Abcam, 52649; 1:200 dilution)—and Alexa-labelled secondary antibodies (Jackson Laboratories, 111-095-003, 115-095-003, 111-025-003 and 115-025-003; 1:500 dilution) with extensive washes. Slides were then mounted with Vectorshield and stained with DAPI (Vector Laboratories). Immunofluorescence images were obtained and analysed using a Nikon Eclipse Ti inverted microscope or a Zeiss LSM710 confocal microscope. A BD FACSCalibur was used for FACS analysis of GFP+ cells according to the manufacturer's instructions.

CRISPR/Cas9-mediated generation of *Her2*$^{-/-}$, *Sting*$^{-/-}$, *Akt1*$^{-/-}$, *Akt2/3*$^{-/-}$ and *Tbk1* knock-in cells. CRISPR–Cas9 genomic editing for gene deletion was performed as described[70]. Guide RNA (gRNA) sequences targeting the *Her2* genomic sequence (hHER2, 5′-CAGCAGAGGATGGAACACAG-3′ and 5′-CTGTGTTCCATCCTCTGCTG-3′; mHER2, 5′-GGGCATGG AGCACCTCCGAG-3′ and 5′-CTCGGAGGTGCTCCATGCCC-3′) were cloned into pX330 plasmids. These constructs together with the puromycin vector pRK7-puromycin were transfected into NMuMG and HCT116 cells at a ratio of 15:1 using the Lipofectamine 3000 transfection reagent. Twenty-four hours after transfection, the cells were selected by puromycin (1.5 µg ml^{-1}) for 72 h and single colonies were obtained by serial dilution and amplification. The STING and AKT1/2/3 primer sequences (hSTING, 5′-ATCCATCCATCCCGTGTCCC-3′ and 5′-GGGACACGGGATGGATGGAT-3′;

hAKT1, 5′-CGTACTCCATGACAAAGCAG-3′ and 5′-CTGCTTTGTCA TGGAGTACG-3′; hAKT2, 5′-TCTCGTCTGGAGAATCCACG-3′ and 5′-CGTGGATTCTCCAGACGAGA-3′; hAKT3, 5′-TTATAATCAGA TGTCTCCAG-3′ and 5′-CTGGGAGACATCTGATTATAA-3′) or the TBK1 FLAG-tag knock-in primer sequences (hTBK1, 5′-AAAGACAGTCAACGTTGCGA-3′ and 5′-TCGCAACGTTGACTGTCTTT-3′) and TBK1 S510A knock-in primer sequences (hTBK1 S510A, 5′-TATTTAGCTTTCCAGTTCTC-3′ and 5′-TTCTATTGTTCCCTGAGAAC-3′) were used to clone the genes into the plasmid gRNA. These constructs were transfected with Cas9-2A–GFP and pMD18 into HCT116 or DLD1 cells. Cells with green fluorescence were then sorted with a flow cytometer (BD FACS Aria II) 36 h after transfection. Clones were identified by immunoblotting with anti-HER2, anti-STING, anti-AKT1/2/3 and anti-FLAG antibodies or digestion/sequencing identification of genomic PCR products. All of the gRNAs used are also listed in Supplementary Table 4.

siRNA-mediated RNA interference. Double stranded small-interfering RNA (siRNA; RiboBio) to silence endogenous HER2 expression in BT474 cells targeted human *Her2* mRNA (sequence: CAGACACGTTTGAGTCCAT). Control siRNA (RiboBio) was used to control for possible non-specific effects of RNA interference. Cells were transfected with siRNA using the Lipofectamine RNAiMAX (Invitrogen) reagent and incubated for 48 h before continuing with the assay and the reverse transfection method was used to reach optimal efficiency. The siRNA sequences are listed in Supplementary Table 4.

Flow cytometry analysis of apoptosis. An Annexin V-FITC/PI apoptosis kit (MultiSciences, AP101) was used to measure apoptotic cells. Briefly, cells treated with hydroxyurea (10 mM) or CPT (1 μM) for 72 h were trypsinized, washed twice with ice-cold PBS and incubated with fluorescent dyes for the flow cytometric analysis according to the manufacturer's manual. The levels of apoptosis were determined using a Beckman CytoFlex. Annexin V- and propidium-iodide-negative cells were considered viable, annexin V-positive but propidium-iodide-negative cells were considered early apoptotic and propidium-iodide-positive cells were considered late apoptotic or dead.

Cellular senescence assays. To evaluate damage-induced cellular senescence, cells at approximately 60–70% confluence were treated for 24 h with hydroxyurea (10 mM), CPT (1 μM) or mitomycin C (1 μM), after which the medium was replaced with fresh medium. The cells were cultured for another 5 d and harvested for the SA-β-Gal assay using a cellular senescence assay kit (Yesen, 40754ES60) according to the manufacturer's manual. Images were acquired using a converted Nikon fluorescence microscope. To detect the SASPs, cells were lysed after 5–8 d of stimulation and subjected to RNA extraction and RT–qPCR assays as described in the previous Methods section to detect the expression of cytokines including MMP12 and IL6, and p21[waf1].

Senescence assays in zebrafish. Zebrafish AB wild-type embryos (male/female) were raised at 28.5 °C in E3 egg water. Forced expression of the ICD of human HER2 was achieved by micro-injection of 25 pg of in-vitro-transcribed mRNA by the mMESSAGE mMACHINE SP6 transcription kit (Life Technology) at the one-cell stage of embryogenesis. At this stage, exogenous mRNAs distribute evenly into most cells by cell division and persist for 72–96 h in the zebrafish embryos. Injected embryos with normal development were selected and used for the senescence study. The embryos were treated with 50 nM CPT from 1.5 to 3.5 d post fertilization and then fixed in 4% paraformaldehyde in PBS at 4 °C. After three washes with PBS (pH 7.4 and pH 6.0) at 4 °C, SA-β-Gal staining was performed according to the manual of the senescence assay kit (Yesen, 40754ES60). The animals were photographed under a dissecting microscope with reflected light. In a parallel experiment, tissue samples of zebrafish embryos at 48 h post fertilization were homogenized, lysed in PBST (1% Triton in PBS) and subjected to SDS–PAGE and immunoblotting. The care of the animals used in experiments was in accordance with the guidelines of and approved by the Laboratory Animal Committee of Zhejiang University. The study is compliant with all relevant ethical regulations regarding animal work.

Murine xenograft growth of B16 melanoma. C57BL/6 wild-type mice were maintained under specific-pathogen-free conditions and randomly selected for tumour injection. Six- to eight-week-old mice were administered a subcutaneous injection of 1.5×10^6 B16-F10 melanoma cells. The injected mice were monitored for tumour growth every day from the ninth day post tumour inoculation, as described in the protocols approved by the IACUC of Zhejiang University. Tumour size is presented as a square caliper measurement and was calculated based on two perpendicular diameters (mm²). The maximum diameter of the tumours was limited to 10 mm, as per the ethical permissions, following which the mice were killed and defined as dead due to tumour burden. To block IFNAR1 by neutralizing antibody, the mice were injected three times intraperitoneally with a single 0.2 mg dose of anti-IFNAR1 antibody (clone MAR1-5A3; BE0241, Bio X Cell) or a mouse IgG1 isotype control (clone MOPC-21; BP0083, Bio X Cell) every other day after the mice had been administered a subcutaneous injection of 1.5×10^6 B16 melanoma cells. The care of the animals used in experiments was in

accordance with guidelines and approved by the Laboratory Animal Committee of Zhejiang University. The study is compliant with all of the relevant ethical regulations regarding animal work.

Murine corneal HSV-1 infection. The right eyes of four- to six-week-old BALB/c mice were infected with 10^6 plaque-forming units of HSV-1 and the left eyes with DMEM without epithelial debridement. PBS containing DMSO (mock) or lapatinib (10 μM) was topically applied to both eyes once a day from the first day post infection. Ocular disease scoring (0–5) was performed in a blinded fashion by two observers based on the following scoring system: 0, no symptoms; 1, mild symptoms with <20% of the eyelid shut; 2, moderate symptoms with 20–50% of the eyelid shut; 3, moderate symptoms with 50–80% of the eyelid shut; 4, severe symptoms with >80% of the eyelid shut and 5, eye completely shut with crusting. The mice were killed at 6 or 9 d.p.i. and their eyeballs were collected for RT–qPCR assays with the HSV-1 primers. BALB/c mice were maintained under specific-pathogen-free conditions and the care of the animals used in experiments was in accordance with the guidelines of and approved by Laboratory Animal Committee of Zhejiang University. The study is compliant with all of the relevant ethical regulations regarding animal work.

Histology and immunohistochemistry. For the histological examinations, mouse tumour samples were dissected, fixed in 4% paraformaldehyde for 12 h at 4 °C, dehydrated in a graded series of ethanol, embedded in paraffin and sliced into 6-μm sections, which were then stained with haematoxylin and eosin. For the immunohistochemistry assays, the tumour samples were dissected, fixed in 4% paraformaldehyde for 12 h at 4 °C, dehydrated overnight with 30% sucrose at 4 °C, embedded in optimal cutting temperature compound and immediately frozen at −80 °C. Samples sectioned at a thickness of 10 μm were washed twice with PBS, permeablized with 0.5% Triton X-100, blocked in 3% horse serum in PBS for 30 min and incubated sequentially with the primary antibodies: anti-CD3 (Abcam, ab16669; 1:100 dilution), anti-CD4 (eBioscience, 14976680; 1:100 dilution), anti-CD8 (eBioscience, 14080880; 1:100 dilution) and anti-F4/80 (Bio-Rad, MCA497RT; 1:100 dilution). After the sections were incubated with Alexa-labelled secondary antibodies (Jackson Laboratories, 111-095-003; 1:500 dilution, Invitrogen, A11006; 1:1000 dilutions) and extensively washed, they were mounted with Vectorshield and stained with DAPI (Vector Laboratories). Immunofluorescence images were obtained and analysed using a Nikon Eclipse Ti inverted microscope or a Zeiss LSM710 confocal microscope.

Nano-liquid chromatography–tandem mass spectrometry analysis. Nanoscale liquid chromatography coupled to tandem mass spectrometry analysis for protein identification, characterization and label-free quantification was performed by Phoenix National Proteomics Core services as previously described[35]. Briefly, tryptic peptides were separated on a C18 column and analysed by LTQ-Orbitrap Velos (Thermo). Proteins were identified using the search engine of the National Center for Biotechnology Information against the human or mouse RefSeq protein databases. The mass spectrometry data of the TBK1 modifications by AKT1 are listed in Supplementary Table 5.

Statistics and reproducibility. Quantitative data are presented as the mean ± s.e.m. from at least three independent experiments. When appropriate, statistically significant differences between multiple comparisons were analysed using the one-way ANOVA test with Bonferroni correction. Differences were considered significant at $P < 0.05$. All samples, if preserved and properly processed, were included in the analyses and no samples or animals were excluded, except for zebrafish with conventional injection damage by pre-established standard. No statistical method was used to predetermine sample sizes and experiments were not randomized, except those involving animals. The investigators were not blinded to allocation during experiments and outcome assessment, except for assessments of the ocular disease score in murine corneal HSV-1 infection.

Reporting Summary. Further information on research design is available in the Nature Research Reporting Summary linked to this article.

Data availability

All data supporting the findings of this study are available in this paper and from the corresponding author on reasonable request. The statistical source data for Figs. 1–7 and Supplementary Figs. 1–7 are provided in Supplementary Table 1, and the source data for Fig. 4e and Supplementary Fig. 4b, that is, the mass spectrometry analysis of the TBK1 modification, is provided in Supplementary Table 5. Mass spectrometry data have been deposited in ProteomeXchange Consortium with the primary accession code PXD013957 via the iProX partner repository.

References

69. Xu, P. et al. Innate antiviral host defense attenuates TGF-β function through IRF3-mediated suppression of Smad signaling. *Mol. Cell* **56**, 723–737 (2014).
70. Ran, F. A. et al. Genome engineering using the CRISPR–Cas9 system. *Nat. Protoc.* **8**, 2281–2308 (2013).

nature research

Corresponding author(s):	Pinglong Xu
Last updated by author(s):	May 17, 2019

Reporting Summary

Nature Research wishes to improve the reproducibility of the work that we publish. This form provides structure for consistency and transparency in reporting. For further information on Nature Research policies, see Authors & Referees and the Editorial Policy Checklist.

Statistics

For all statistical analyses, confirm that the following items are present in the figure legend, table legend, main text, or Methods section.

n/a	Confirmed	
☐	☒	The exact sample size (*n*) for each experimental group/condition, given as a discrete number and unit of measurement
☐	☒	A statement on whether measurements were taken from distinct samples or whether the same sample was measured repeatedly
☐	☒	The statistical test(s) used AND whether they are one- or two-sided *Only common tests should be described solely by name; describe more complex techniques in the Methods section.*
☒	☐	A description of all covariates tested
☐	☒	A description of any assumptions or corrections, such as tests of normality and adjustment for multiple comparisons
☐	☒	A full description of the statistical parameters including central tendency (e.g. means) or other basic estimates (e.g. regression coefficient) AND variation (e.g. standard deviation) or associated estimates of uncertainty (e.g. confidence intervals)
☒	☐	For null hypothesis testing, the test statistic (e.g. *F*, *t*, *r*) with confidence intervals, effect sizes, degrees of freedom and *P* value noted *Give P values as exact values whenever suitable.*
☒	☐	For Bayesian analysis, information on the choice of priors and Markov chain Monte Carlo settings
☒	☐	For hierarchical and complex designs, identification of the appropriate level for tests and full reporting of outcomes
☒	☐	Estimates of effect sizes (e.g. Cohen's *d*, Pearson's *r*), indicating how they were calculated

Our web collection on statistics for biologists contains articles on many of the points above.

Software and code

Policy information about availability of computer code

Data collection	Commercial softwares equipped by CentroLIA LB 961 (Berthold Tech), CFX96 real-time PCR (CFX Manager, Bio-Rad), LSM710 confocal microscope (ZEN 2.1, Zeiss), Eclipse Ti (Nikon), SMZ18 (Nikon), FACSCalibur (CellQuest Pro 6.0, BD), and CytoFlex (Beckman).
Data analysis	Analyzed by SigmaPlot 10.0, Orgin Pro 9.1, GraphPad Prism 5.01, ZEN 2010, CytExpert 2.3, CellQuest Pro 6.0, Microsoft Excel 2013, and Adobe Photoshop 7.0.

For manuscripts utilizing custom algorithms or software that are central to the research but not yet described in published literature, software must be made available to editors/reviewers. We strongly encourage code deposition in a community repository (e.g. GitHub). See the Nature Research guidelines for submitting code & software for further information.

Data

Policy information about availability of data

All manuscripts must include a data availability statement. This statement should provide the following information, where applicable:

- Accession codes, unique identifiers, or web links for publicly available datasets
- A list of figures that have associated raw data
- A description of any restrictions on data availability

Source data for supporting the findings of this study are provided in the paper, and/or available from the corresponding author on reasonable request. Statistical source data for Figs. 1-7 and Supplementary Figs. 1-7 are provided in Supplementary Table 1.

Field-specific reporting

Please select the one below that is the best fit for your research. If you are not sure, read the appropriate sections before making your selection.

☒ Life sciences   ☐ Behavioural & social sciences   ☐ Ecological, evolutionary & environmental sciences

For a reference copy of the document with all sections, see nature.com/documents/nr-reporting-summary-flat.pdf

Life sciences study design

All studies must disclose on these points even when the disclosure is negative.

Sample size	According to standards in the field and the experimental experience and knowledge to choose an adequate pool for reporter assay, RT-qPCR, FACS, microscopy, and mice and zebrafish experiments. No statistical method was used to predetermine sample size.
Data exclusions	No exclusion except for zebrafish that have injury and died within 6 hours of microinjection, by the pre-established exclusion criteria for conventional injection damage (5%-10% rate). Stated in Methods section of zebrafish experiment.
Replication	For each representative image/data, experiments were performed at least three times with similar results unless otherwise noted in the manuscript. Stated in the Methods section.
Randomization	A simple randomization method was used to allocate the experimental groups of mice and zebrafish. Stated in the Methods section.
Blinding	All samples were not blinded in this study, except in assessing the ocular disease score. Blind experiments were not necessary as all measurements except ocular disease scores were objective.

Reporting for specific materials, systems and methods

We require information from authors about some types of materials, experimental systems and methods used in many studies. Here, indicate whether each material, system or method listed is relevant to your study. If you are not sure if a list item applies to your research, read the appropriate section before selecting a response.

Materials & experimental systems

n/a	Involved in the study
☐	☒ Antibodies
☐	☒ Eukaryotic cell lines
☒	☐ Palaeontology
☐	☒ Animals and other organisms
☒	☐ Human research participants
☒	☐ Clinical data

Methods

n/a	Involved in the study
☒	☐ ChIP-seq
☐	☒ Flow cytometry
☒	☐ MRI-based neuroimaging

Antibodies

Antibodies used	Stated in the Methods section. Antibody information is provided in the separate Supplementary Table 3 for the source, catalog numbers,clone numbers and dilution ratio of antibodies in distinct applications.
Validation	Validation of antibodies, including the contents of the species and application, are provided by individual commercial providers including CST Biotech, Abcam, Sigma, eBioscience, BD Bioscience, and Bio-Rad in their user manuals and websites, and according to previous publications as well as validated by the use of negative and/or positive controls. Stated in the Methods section for validation of antibodies.

Eukaryotic cell lines

Policy information about cell lines

Cell line source(s)	Cell lines (NMuMG, HCT116, DLD1, HEK293, B16-F10, and MEF) were from ATCC; BT474 and SKBR-3 cells were obtained from Cell Bank (CAS Collection Committee, Shanghai); mouse peritoneal macrophages (PMs) were obtained from mice and human peripheral blood mononuclear cells (PBMCs) were obtained from healthy blood, according to standard protocols. Stated in the Methods section.
Authentication	The cell lines were not authenticated. Stated in the Methods section.
Mycoplasma contamination	All cell lines were tested negative for mycoplasma contamination. Stated in the Methods section.

| Commonly misidentified lines
(See ICLAC register) | No cell lines used in this study were found in the database of commonly misidentified cell lines that is maintained by ICLAC and NCBI Biosample. Stated in the Methods section. |

Animals and other organisms

Policy information about studies involving animals; ARRIVE guidelines recommended for reporting animal research

Laboratory animals	The zebrafish (Danio rerio), AB wild-type strain, male/female, embryo from the one-cell stage of embryogenesis to 120 hpf. The mice, C57BL/6, male, 6-8 weeks old; BALB/c mice, male, 4-6 weeks old.
Wild animals	Wild animals were not involved in this study.
Field-collected samples	Samples collected from the field were not involved in this study.
Ethics oversight	Care of experimental animals was in accordance with guidelines and approved by the Laboratory Animal Committee of Zhejiang University.

Note that full information on the approval of the study protocol must also be provided in the manuscript.

Flow Cytometry

Plots

Confirm that:

☒ The axis labels state the marker and fluorochrome used (e.g. CD4-FITC).

☒ The axis scales are clearly visible. Include numbers along axes only for bottom left plot of group (a 'group' is an analysis of identical markers).

☐ All plots are contour plots with outliers or pseudocolor plots.

☒ A numerical value for number of cells or percentage (with statistics) is provided.

Methodology

Sample preparation	Analysis or sorting of cells by flow cytometry was described in the Methods section. Briefly, cells with indicated treatment were trypsinized, washed twice with ice-cold PBS, (or) incubated with fluorescent dyes, and subjected to analysis or sorting according to manufacturer manuals.
Instrument	FACSCalibur (BD) for infection assays, CytoFlex (Beckman) for apoptosis assays, FACS Aria II (BD) for cell sorting in CRISPR-based applications.
Software	CytExpert 2.3 (Beckman), CellQuest Pro 6.0 (BD), and FACSDiva 6.0 (BD),
Cell population abundance	In analyzing of viral infection or apoptosis, a typical population of 10k was used. For the generation of knockout/knock-in cells by CRISPR, post-sorting cells were planted as single and propagated, verified by protein expression by immunoblotting or PCR and sequencing of genomic DNA. See Method section and Figures 5A, 5C, 5F, and 6H for cell proportions and purity.
Gating strategy	Preliminary FSC/SSC gating was selected by the scatter plots of normal cell population, and gate boundaries were determined by the positive/negative control and based on experience.

☐ Tick this box to confirm that a figure exemplifying the gating strategy is provided in the Supplementary Information.